Effect of the alkyl linker length on the photoisomerization of hydrazone switches on metal surfaces

Author(s):
Zheng, Liqing; Yang, Sirun; Krähenbühl, Sven; Rybkin, Vladimir V.; Lan, Jinggang; Aprahamian, Ivan; Zenobi, Renato

Publication date:
2022-06

Permanent link:
https://doi.org/10.3929/ethz-b-000531705

Originally published in:
Materials Today Chemistry 24, https://doi.org/10.1016/j.mtchem.2022.100797

Funding acknowledgement:
741431 - Nanoscale Vibrational Spectroscopy of Sensitive 2D Molecular Materials (EC)

Supporting information

Effect of the alkyl linker length on the photoisomerization of hydrazone switches on metal surfaces

Li-Qing Zheng[a+], Sirun Yang[b+], Sven Krähenbühl[a], Vladimir V. Rybkin[c], Jinggang Lan[c*], Ivan Aprahamian[b*] and Renato Zenobi[a*]

a. Department of Chemistry and Applied Biosciences, ETH Zurich, Vladimir-Prelog-Weg 3, CH 8093, Switzerland

b. Department of Chemistry, Dartmouth College, Hanover, New Hampshire 03755, United States

c. Department of Chemistry, University of Zurich, Winterthurerstrasse 190, CH 8057, Switzerland

Table of Contents

1. Chemical synthesis

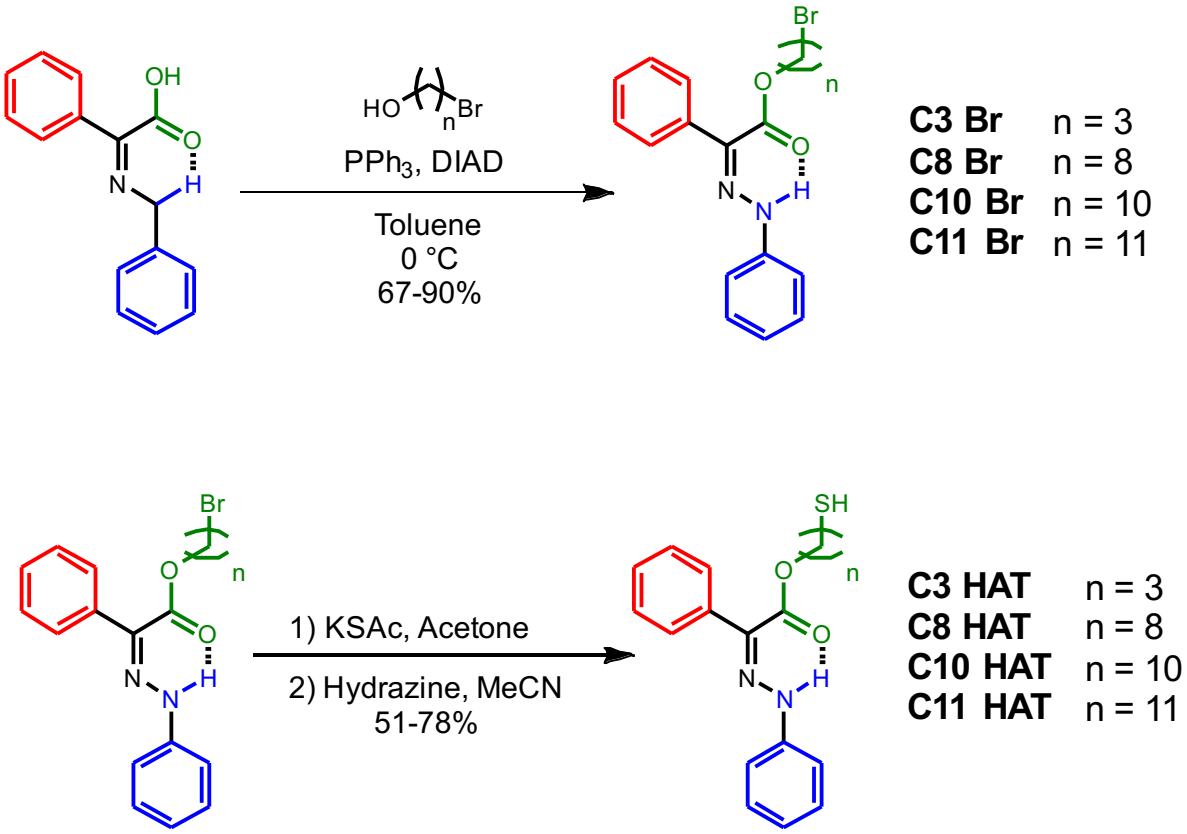

Scheme S1. Synthesis of **Cn HAT** and model compound **Cn Br**

Both **Cn HAT** and model compound **Cn Br** (**Scheme S1**) were synthesized using a reported procedure.[S1]

Chemical Formula: $C_{15}H_{13}BrN_2O_2$

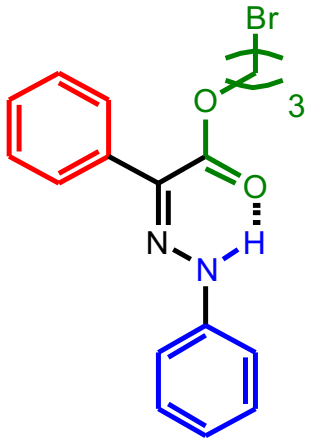

C3 Br

C3 Br was obtained as a yellow solid; yield 67 %. m.p. 82.5 – 83.5 °C. ^{1}H NMR (600 MHz, CD_2Cl_2) δ 12.35 (s, 1H), 7.63 (d, J = 8.0 Hz, 2H), 7.39 (t, J = 7.6 Hz, 2H), 7.33 (t, J = 8.0 Hz, 3H), 7.29 (d, J = 8.2 Hz, 2H), 7.01 (t, J = 7.1 Hz, 1H), 4.43 (t, J = 6.1 Hz, 2H), 3.46 (t, J = 6.4 Hz, 2H), 2.25 (p, J = 6.3 Hz, 2H) ppm. ^{13}C NMR (151 MHz, CD_2Cl_2) δ 163.94, 143.80, 137.11, 129.91, 129.13, 128.56, 128.43, 128.17, 123.13, 114.77, 63.26, 31.91, 30.23 ppm. Hi-Res ESI-MS: *m/z* found [M-H$^+$] for $C_{17}H_{18}N_2O_2Br^+$ 361.0545 (calcd. 361.0552).

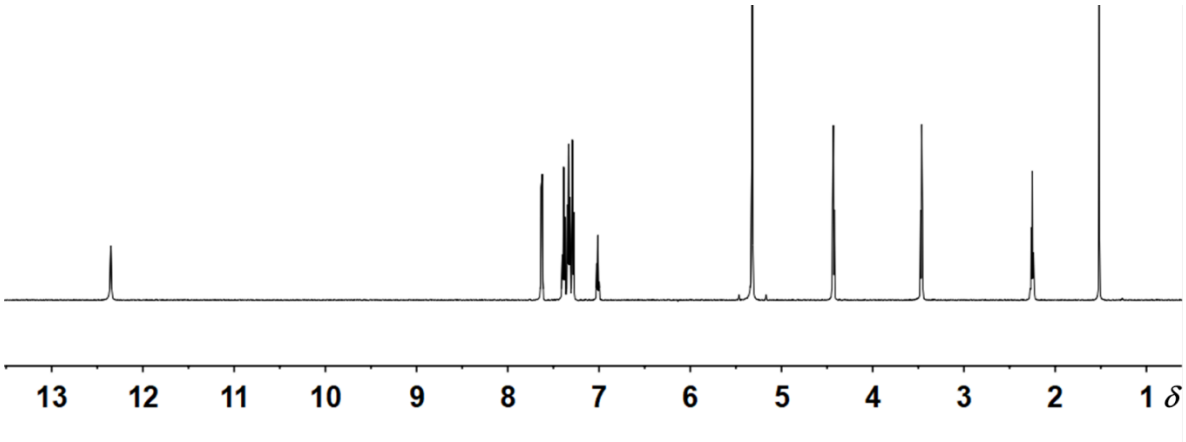

Figure S1. ^{1}H NMR spectrum of **C3 Br** in CD_2Cl_2 at 298 K

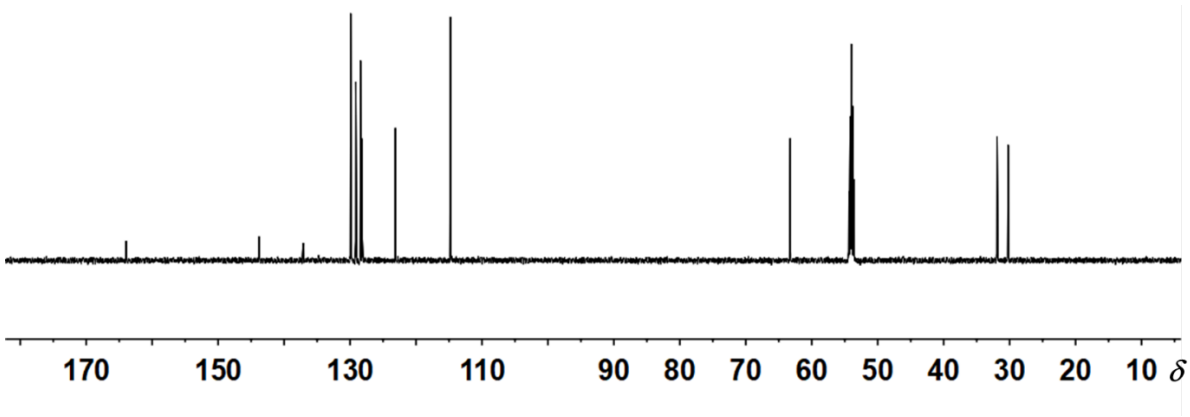

Figure S2. ^{13}C NMR spectrum of **C3 Br** in CD_2Cl_2 at 298 K

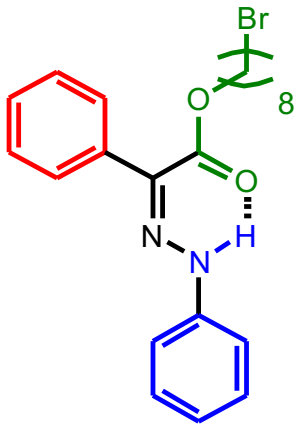

C8 Br

C8 Br was obtained as yellow oil; yield 80 %. ^1H NMR (600 MHz, CD_2Cl_2) δ 12.36 (s, 1H), 7.65 (d, J = 7.8 Hz, 2H), 7.38 (t, J = 7.5 Hz, 2H), 7.33 (t, J = 7.8 Hz, 3H), 7.28 (d, J = 8.2 Hz, 2H), 7.00 (t, J = 7.2 Hz, 1H), 4.29 (t, J = 6.7 Hz, 2H), 3.42 (t, J = 6.9 Hz, 2H), 1.89 – 1.78 (m, 2H), 1.75 – 1.65 (m, 2H), 1.45 – 1.30 (m, 8H). ^{13}C NMR (151 MHz, CD_2Cl_2) δ 164.25, 143.93, 137.23, 129.90, 129.19, 128.87, 128.35, 128.09, 122.94, 114.67, 65.76, 34.74, 33.39, 29.51, 29.15, 28.96, 28.59, 26.48 ppm. Hi-Res ESI-MS: *m/z* found [M-H$^+$] for $C_{22}H_{28}N_2O_2Br^+$ 431.1322 (calcd. 431.1334).

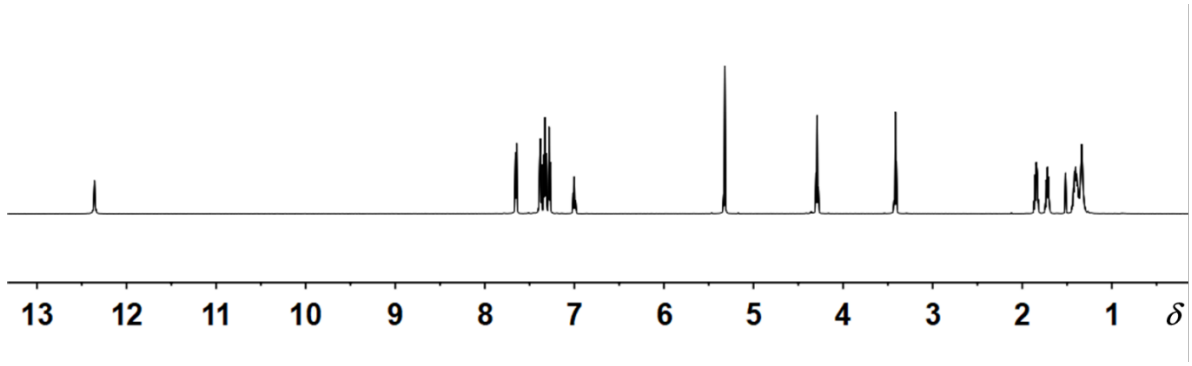

Figure S3. ^1H NMR spectrum of **C8 Br** in CD_2Cl_2 at 298 K

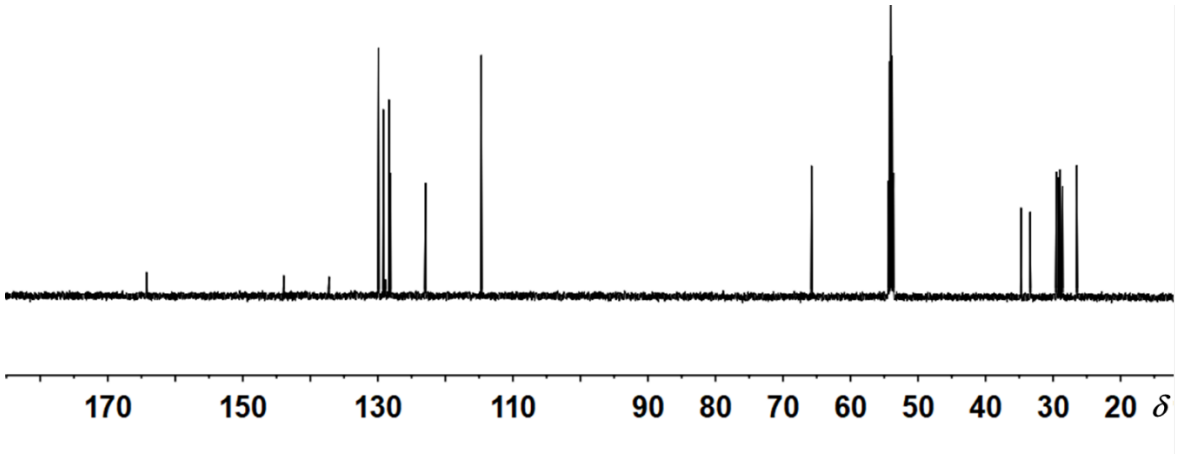

Figure S4. ^{13}C NMR spectrum of **C8 Br** in CD_2Cl_2 at 298 K

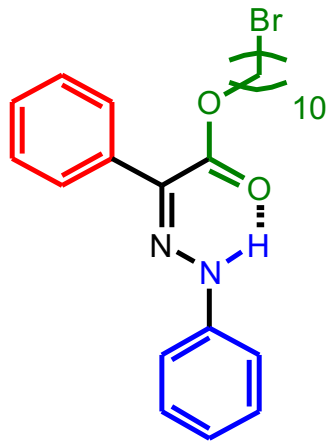

C10 Br

C10 Br was obtained as yellow oil; yield 77 %. ^1H NMR (600 MHz, CD_2Cl_2) δ 12.35 (s, 1H), 7.65 (d, J = 7.7 Hz, 2H), 7.38 (t, J = 7.4 Hz, 2H), 7.33 (t, J = 7.5 Hz, 3H), 7.28 (d, J = 8.0 Hz, 2H), 7.00 (t, J = 7.1 Hz, 1H), 4.29 (t, J = 6.6 Hz, 2H), 3.42 (t, J = 6.8 Hz, 2H), 1.88 – 1.81 (m, 2H), 1.75 – 1.68 (m, 2H), 1.44 – 1.27 (m, 12H) ppm. ^{13}C NMR (151 MHz, CD_2Cl_2) δ 164.25, 143.93, 137.23, 129.90, 129.19, 128.89, 128.35, 128.09, 122.93, 114.67, 65.81, 34.81, 33.46, 29.92, 29.86, 29.65, 29.28, 29.00, 28.71, 26.56 ppm. Hi-Res ESI-MS: *m/z* found [M-H$^+$] for $C_{24}H_{32}N_2O_2Br^+$ 459.1650 (calcd. 459.1647).

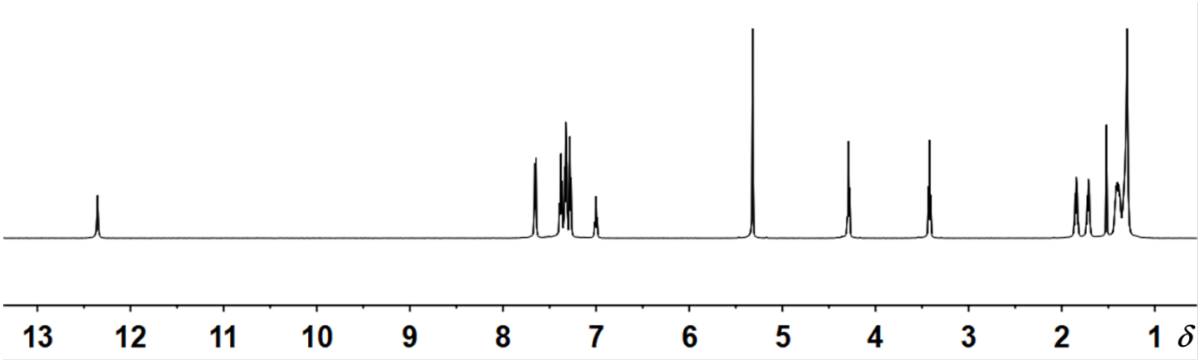

Figure S5. ^{1}H NMR spectrum of **C10 Br** in CD_2Cl_2 at 298 K

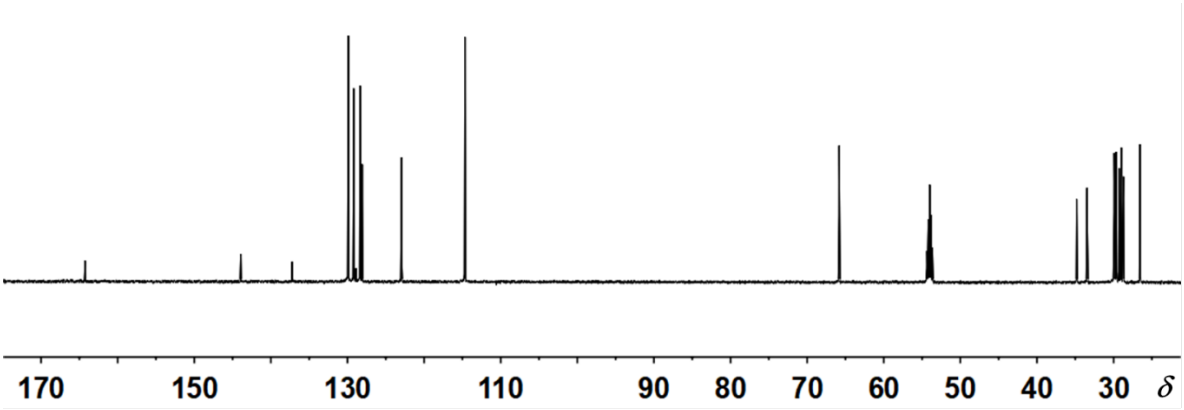

Figure S6. ^{13}C NMR spectrum of **C10 Br** in CD_2Cl_2 at 298 K

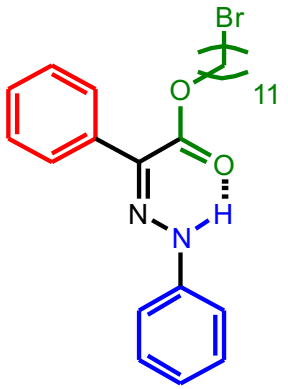

C11 Br

C11 Br was obtained as yellow oil; yield 90 %. ^{1}H NMR (600 MHz, CD_2Cl_2) δ 12.36 (s, 1H), 7.65 (d, J = 7.4 Hz, 2H), 7.38 (t, J = 7.4 Hz, 2H), 7.33 (t, J = 7.6 Hz, 3H), 7.28 (d, J = 7.8 Hz, 2H), 7.00 (t, J = 7.1 Hz, 1H), 4.29 (t, J = 6.6 Hz, 2H), 3.42 (t, J = 6.8 Hz, 2H), 1.88 – 1.80 (m, 2H), 1.76 – 1.67 (m, 2H), 1.45 – 1.25 (m, 14H) ppm. ^{13}C NMR (151 MHz, CD_2Cl_2) δ 164.26, 143.94, 137.23, 129.90, 129.19, 128.89, 128.35, 128.08, 122.93, 114.67, 65.83, 34.83, 33.47, 29.99, 29.96, 29.69, 29.31, 29.00, 28.73, 26.57 ppm. Hi-Res ESI-MS: *m/z* found [M-H^{+}] for $C_{25}H_{34}N_2O_2Br^{+}$ 473.1799 (calcd. 473.1804)

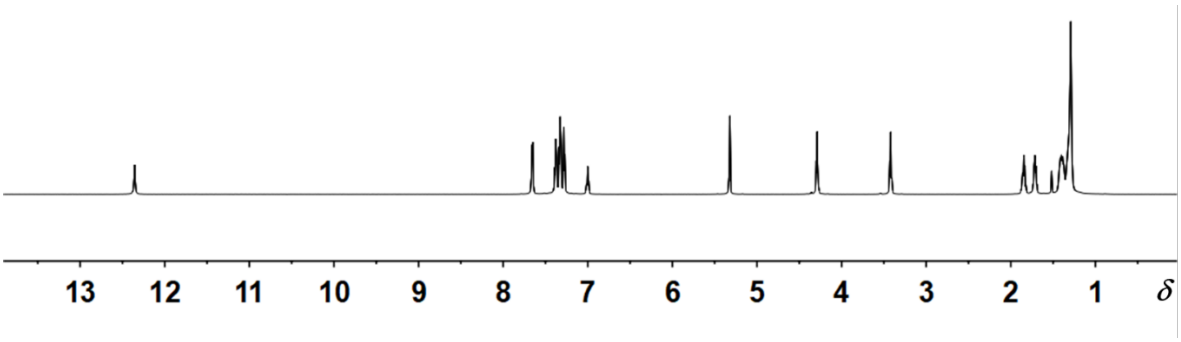

Figure S7. ^{1}H NMR spectrum of **C11 Br** in CD_2Cl_2 at 298 K

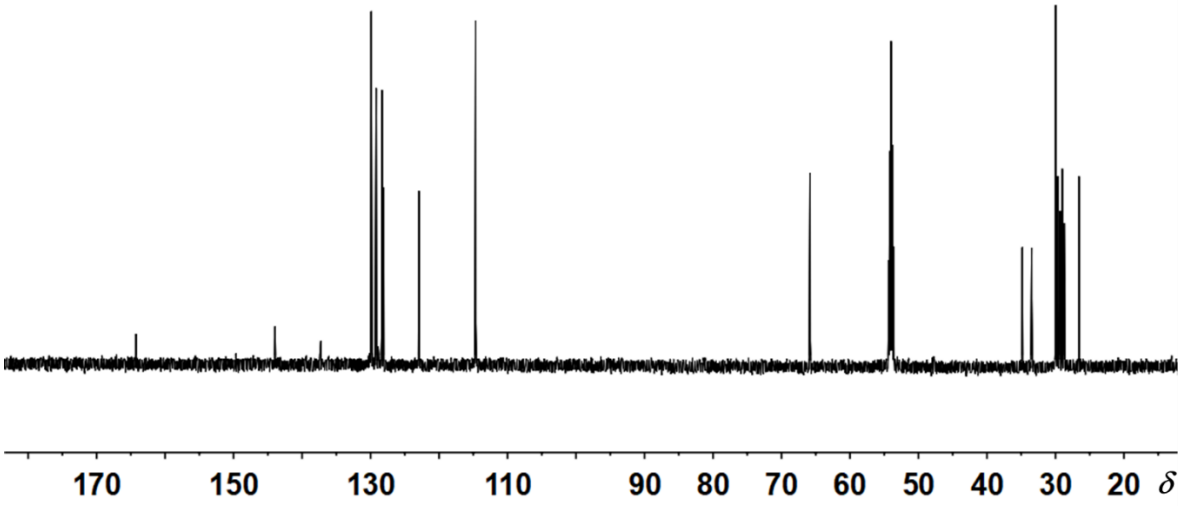

Figure S8. ^{13}C NMR spectrum of **C11 Br** in CD_2Cl_2 at 298 K

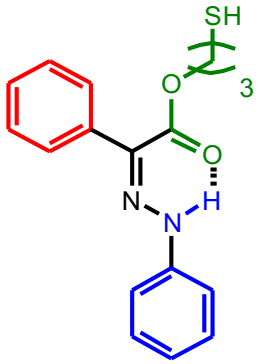

C3 HAT

C3 HAT was obtained as a yellow solid; yield 51 %. m.p. 96.8 – 97.5 °C. ^{1}H NMR (500 MHz, CD_2Cl_2) δ 12.36 (s, 1H), 7.65 – 7.61 (m, 2H), 7.41 – 7.36 (m, 2H), 7.36 – 7.30 (m, 3H), 7.30 – 7.26 (m, 2H), 7.01 (tt, J = 7.3, 1.3 Hz, 1H), 4.41 (dd, J = 7.9, 4.5 Hz, 2H), 2.60 (dt, J = 8.0, 7.0 Hz, 2H), 2.01 (dt, J = 9.6, 6.6 Hz, 2H), 1.45 (t, J = 8.2 Hz, 1H) ppm. ^{13}C NMR (151 MHz, CD_2Cl_2) δ 164.08, 143.84, 137.14, 129.91, 129.15, 128.56, 128.41, 128.15, 123.07, 114.74, 63.60, 33.14, 21.69 ppm. Hi-Res ESI-MS: *m/z* found [M-H$^+$] for $C_{17}H_{19}N_2O_2S^+$ 315.1169 (calcd. 315.1167).

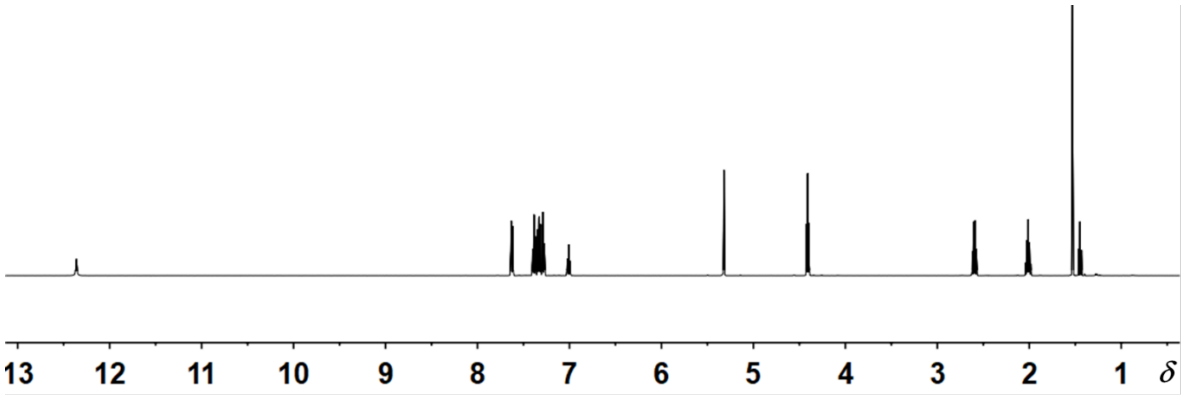

Figure S9. ^{1}H NMR spectrum of **C3 HAT** in CD_2Cl_2 at 298 K

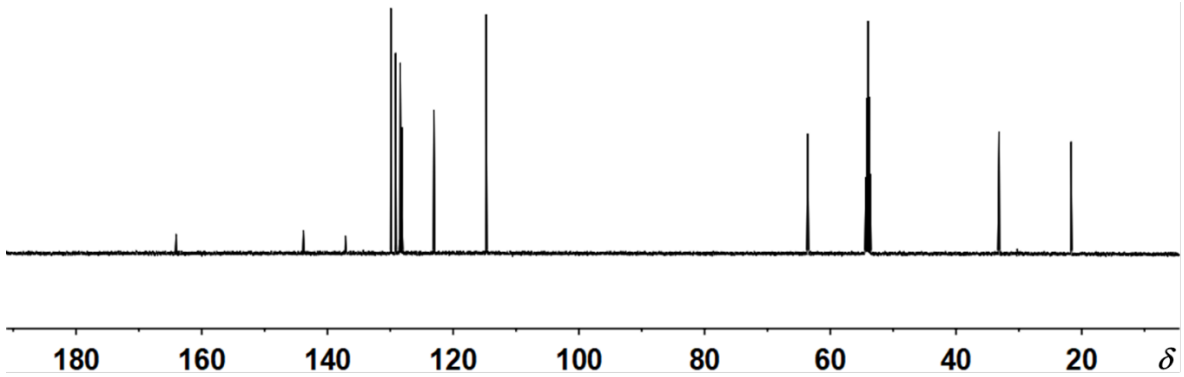

Figure S10. ^{13}C NMR spectrum of **C3 HAT** in CD_2Cl_2 at 298 K

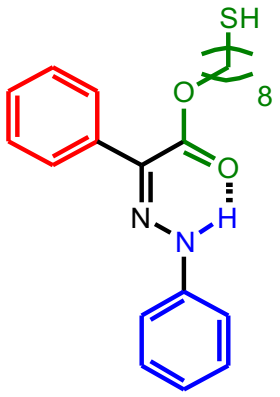

C8 HAT

C8 HAT was obtained as yellow oil; yield 60 %. ^{1}H NMR (600 MHz, CD_2Cl_2) δ 12.35 (s, 1H), 7.65 (d, J = 8.0 Hz, 2H), 7.38 (t, J = 7.6 Hz, 2H), 7.33 (t, J = 7.6 Hz, 3H), 7.28 (d, J = 8.2 Hz, 2H), 7.00 (t, J = 7.2 Hz, 1H), 4.29 (t, J = 6.6 Hz, 2H), 2.54 – 2.46 (m, 2H), 1.76 – 1.67 (m, 2H), 1.59 (dt, J = 14.9, 7.3 Hz, 2H), 1.41 – 1.29 (m, 9H) ppm. ^{13}C NMR (151 MHz, CD_2Cl_2) δ 164.25, 143.93, 137.23, 129.90, 129.19, 128.88, 128.35, 128.09, 122.94, 114.67, 65.78, 34.63, 29.58, 29.46, 28.97, 28.79, 26.51, 25.09 ppm. Hi-Res ESI-MS: *m/z* found [M-H^{+}] for $C_{22}H_{29}N_2O_2S^{+}$ 385.1945 (calcd. 385.1950).

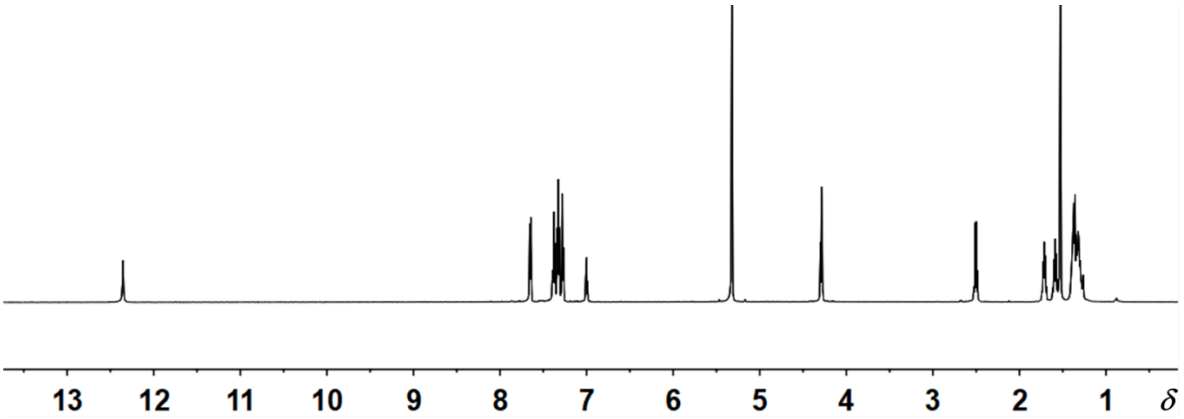

Figure S11. ^{1}H NMR spectrum of **C8 HAT** in CD_2Cl_2 at 298 K

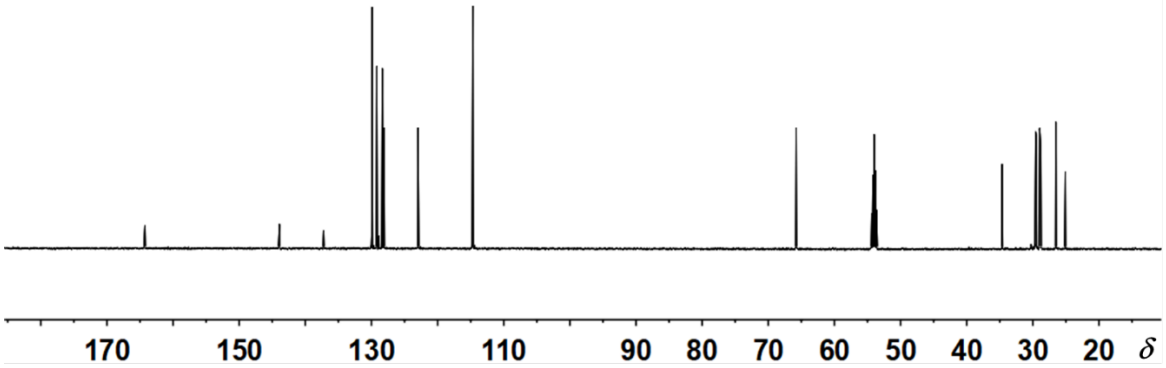

Figure S12. ^{13}C NMR spectrum of **C8 HAT** in CD_2Cl_2 at 298 K

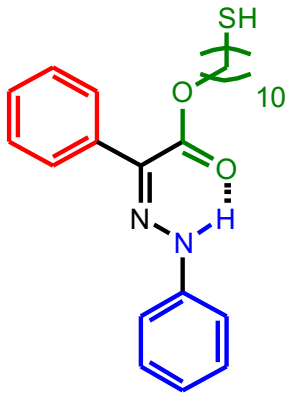

C10 HAT

C10 HAT was obtained as yellow oil; yield 71 %. ^{1}H NMR (600 MHz, CD_2Cl_2) δ 12.37 (s, 1H), 7.66 (d, J = 7.9 Hz, 2H), 7.39 (t, J = 7.5 Hz, 2H), 7.33 (dd, J = 15.8, 8.0 Hz, 3H), 7.28 (d, J = 8.1 Hz, 2H), 7.01 (t, J = 7.2 Hz, 1H), 4.29 (t, J = 6.7 Hz, 2H), 2.51 (q, J = 7.4 Hz, 2H), 1.77 – 1.67 (m, 2H), 1.65 – 1.55 (m, 2H), 1.45 – 1.24 (m, 13H) ppm. ^{13}C NMR (151 MHz, CD_2Cl_2) δ 164.25, 143.93, 137.23, 129.90, 129.19, 128.89, 128.35, 128.09, 122.93, 114.67, 65.81, 34.81, 33.46, 29.92, 29.86, 29.65, 29.28, 29.00, 28.71, 26.56 ppm. Hi-Res ESI-MS: *m/z* found [M-H^{+}] for $C_{24}H_{33}N_2O_2S^{+}$ 413.2269 (calcd. 413.2263).

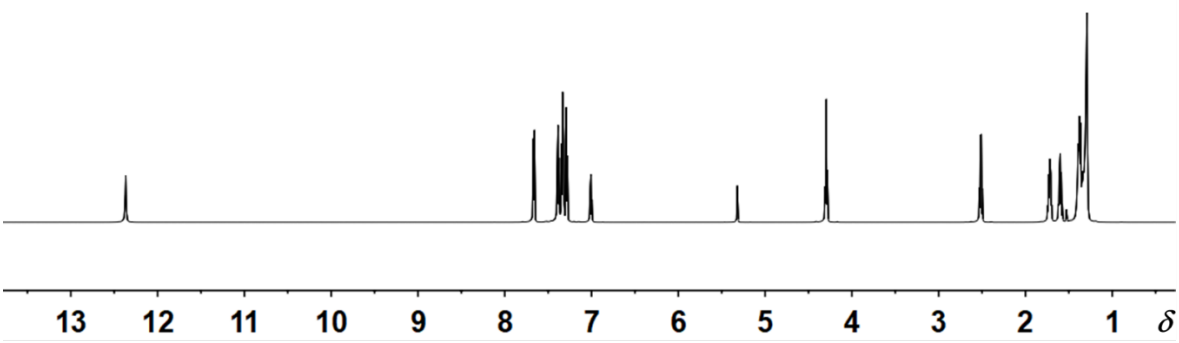

Figure S13. ^{1}H NMR spectrum of **C10 HAT** in CD_2Cl_2 at 298 K

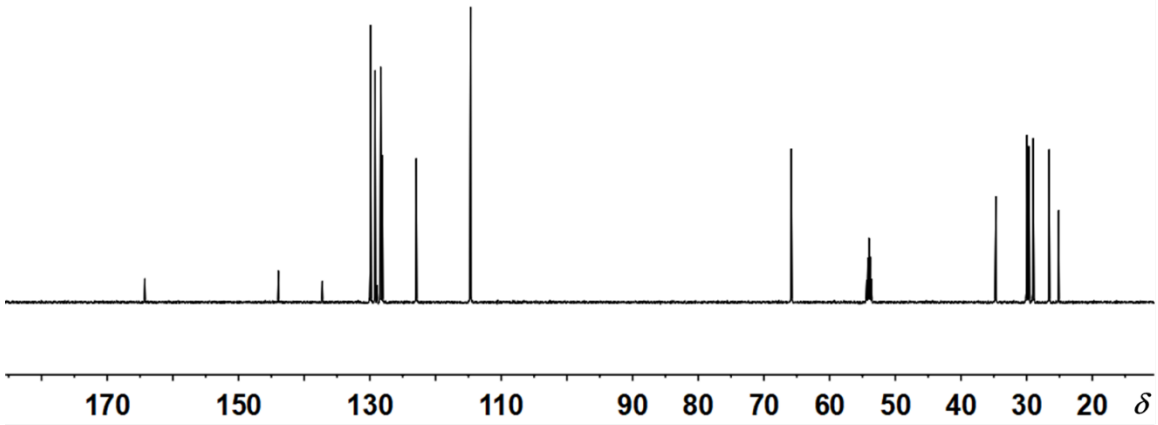

Figure S14. ^{13}C NMR spectrum of **C10 HAT** in CD_2Cl_2 at 298 K

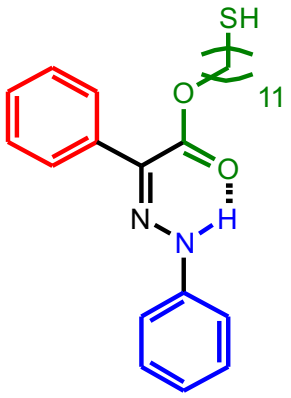

C11 HAT

C11 HAT was obtained as yellow oil; yield 78 %. ^{1}H NMR (600 MHz, CD_2Cl_2) δ 12.39 (s, 1H), 7.72 – 7.66 (m, 2H), 7.41 (t, *J* = 7.4 Hz, 2H), 7.36 (t, *J* = 7.7 Hz, 3H), 7.31 (d, *J* = 7.6 Hz, 2H), 7.04 (t, *J* = 7.2 Hz, 1H), 4.33 (t, *J* = 6.7 Hz, 2H), 2.54 (dd, *J* = 14.8, 7.5 Hz, 2H), 1.79 – 1.71 (m, 2H), 1.67 – 1.60 (m, 2H), 1.47 – 1.27 (m, 15H) ppm. ^{13}C NMR (151 MHz, CD_2Cl_2) *δ* 164.26, 143.93, 137.23, 129.89, 129.19, 128.89, 128.35, 128.08, 122.93, 114.66, 65.83, 34.70, 30.26, 30.05, 30.01, 29.69, 29.63, 29.00, 28.93, 26.57, 25.12 ppm. Hi-Res ESI-MS: *m/z* found [M-H^{+}] for $C_{25}H_{35}N_2O_2S^{+}$ 427.2421 (calcd. 427.2419).

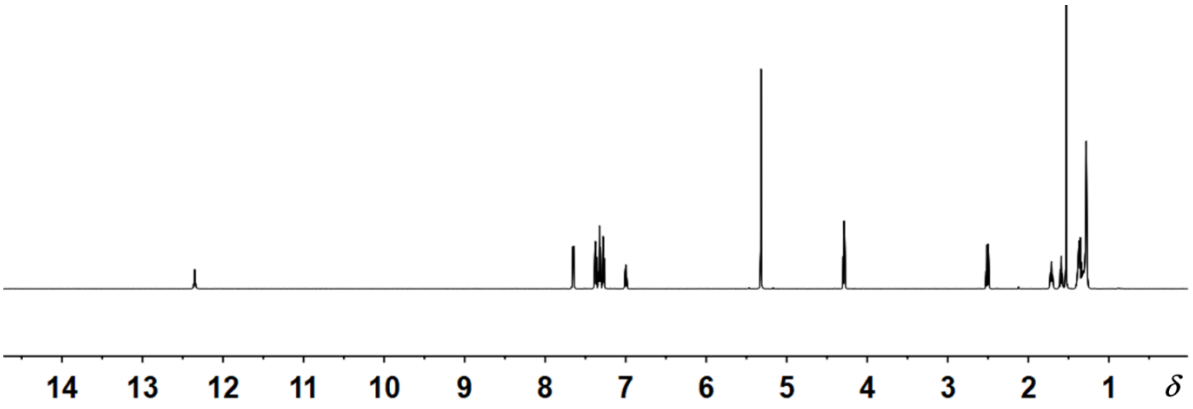

Figure S15. ^{1}H NMR spectrum of **C11 HAT** in CD_2Cl_2 at 298 K

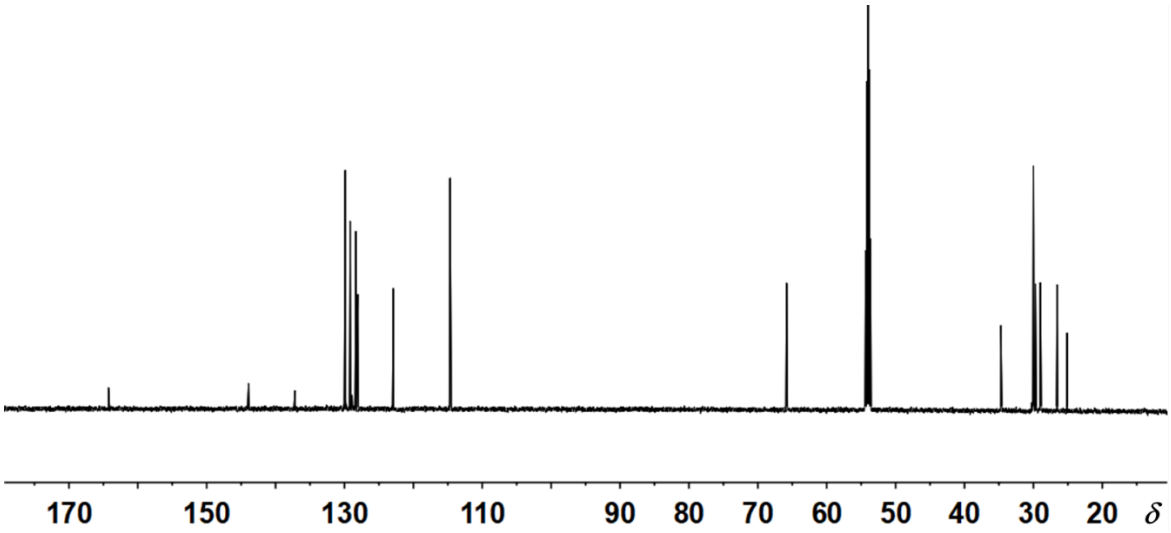

Figure S16. ^{13}C NMR spectrum of **C11 HAT** in CD_2Cl_2 at 298 K

3. Photoisomerization studies in toluene solution

UV/Vis and ^{1}H NMR spectroscopies were employed to study the photoisomerization in solution. A **Cn HAT** toluene solution (3.0 mL, 1.0×10^{-5} M) was prepared and transferred into a 1.0 cm quartz cuvette for immediate UV/Vis absorption measurements. The solution was then irradiated, and the change in UV spectra recorded. Isomerization cycles were measured by alternating the irradiation wavelength between the appropriate values and monitoring the change in UV/Vis absorption spectra. The photostationary states (PSS) were determined upon continuous irradiation of the sample until no further isomerization was observed using ^{1}H NMR spectroscopy.

2. Photoisomerization studies in toluene solution

2.1 UV-Vis spectroscopy analysis

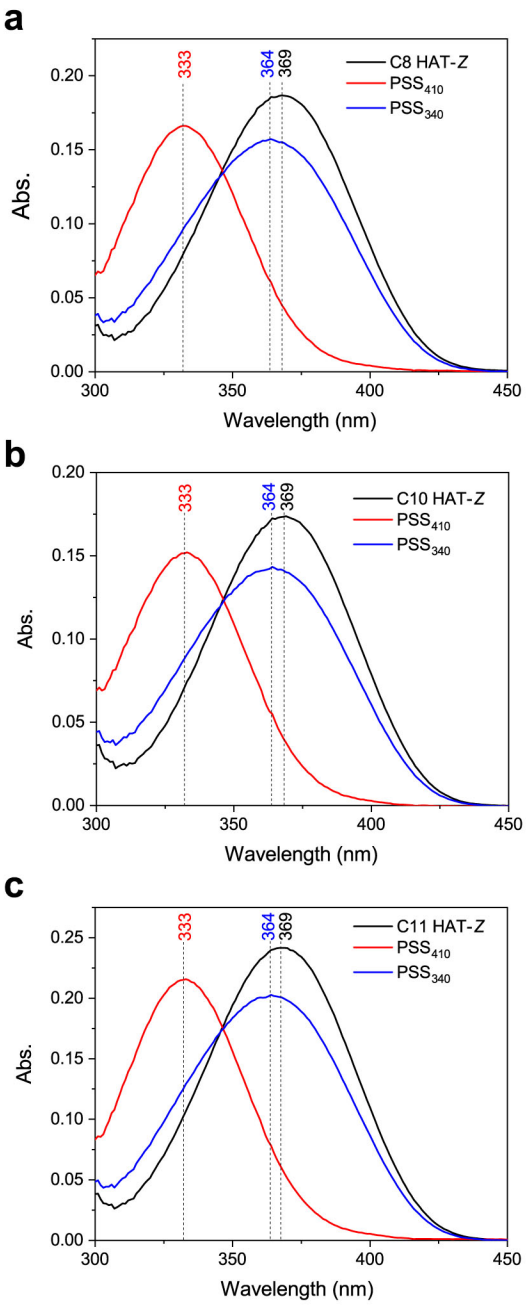

Figure S17. UV-vis spectra of Cn HAT in toluene (1×10^{-5} M) before (black curve) and after irradiation with 410 nm light (red curve), followed by irradiation with 340 nm light (blue curve), (**a**). C8 HAT; (**b**). C10 HAT; (**c**). C11 HAT.

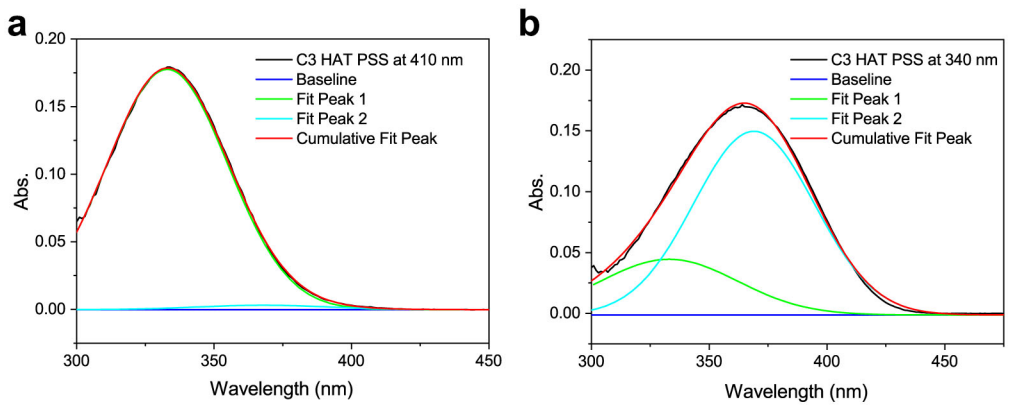

Figure S18. Gaussian curve fit of the UV-vis spectrum of C3 HAT in toluene after irradiation with 410 nm light (**a**), followed by irradiation with 340 nm light (**b**).

Table S1. Photochemical properties of Cn HAT (n = 3, 8, 10, 11) in toluene

Parameter	C3 HAT	C8 HAT	C10 HAT	C11 HAT
$\lambda_{max,\ Z\ isomer}$ (nm)	369	369	369	369
$\lambda_{max,\ PSS\ 415}$ (nm)	333	333	333	333
$([E]:[Z])_{PSS415}$ (%)	98:2	98:2	98:2	98:2
$\lambda_{max,\ PSS\ 340}$ (nm)	364	364	364	364
$([E]:[Z])_{PSS340}$ (%)	23:77	23:77	23:77	23:77

2.2 NMR quantitative analysis

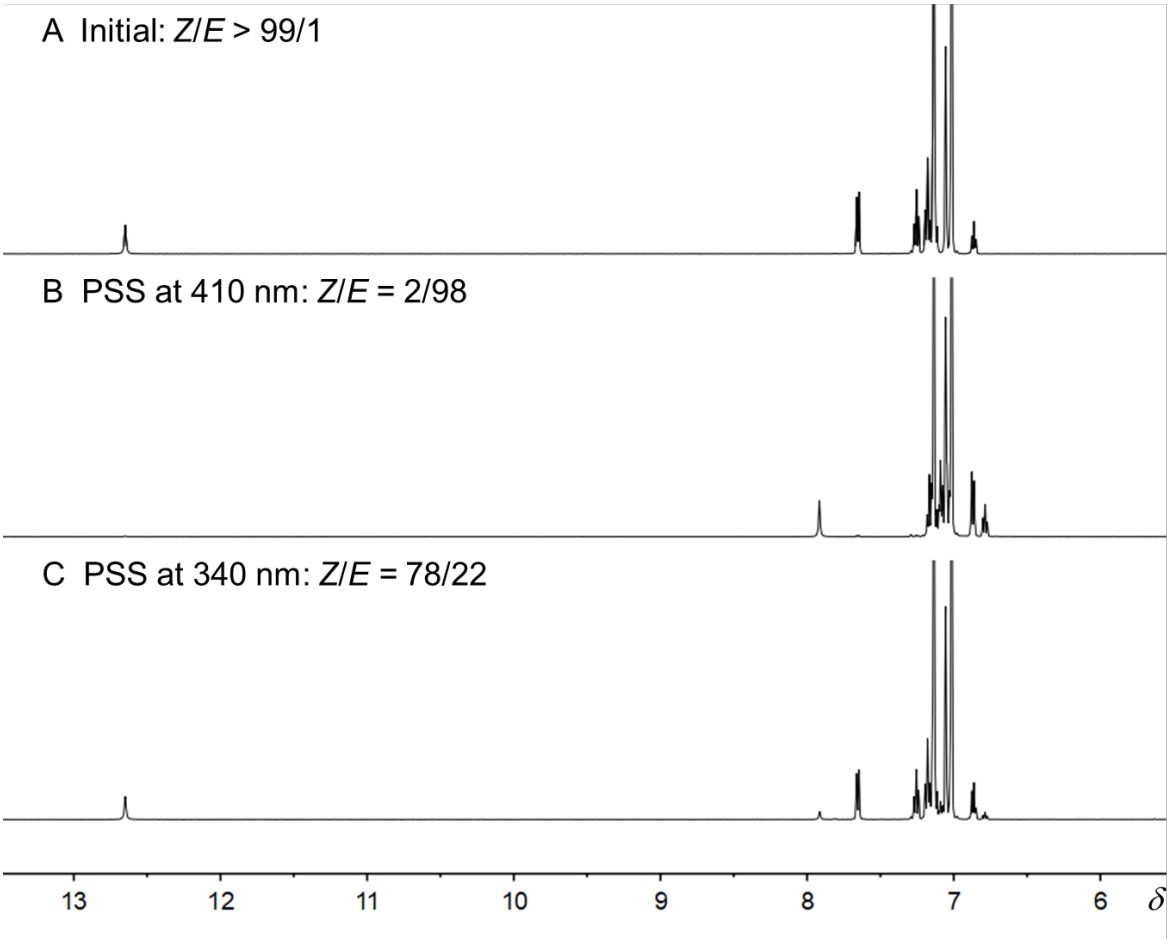

Figure S19. ^{1}H NMR spectra (toluene-d_8, 298 K) of **C3 HAT** (A) before, and after (B) 410 nm followed by (C) 340 nm photo irradiation to reach the PSS.

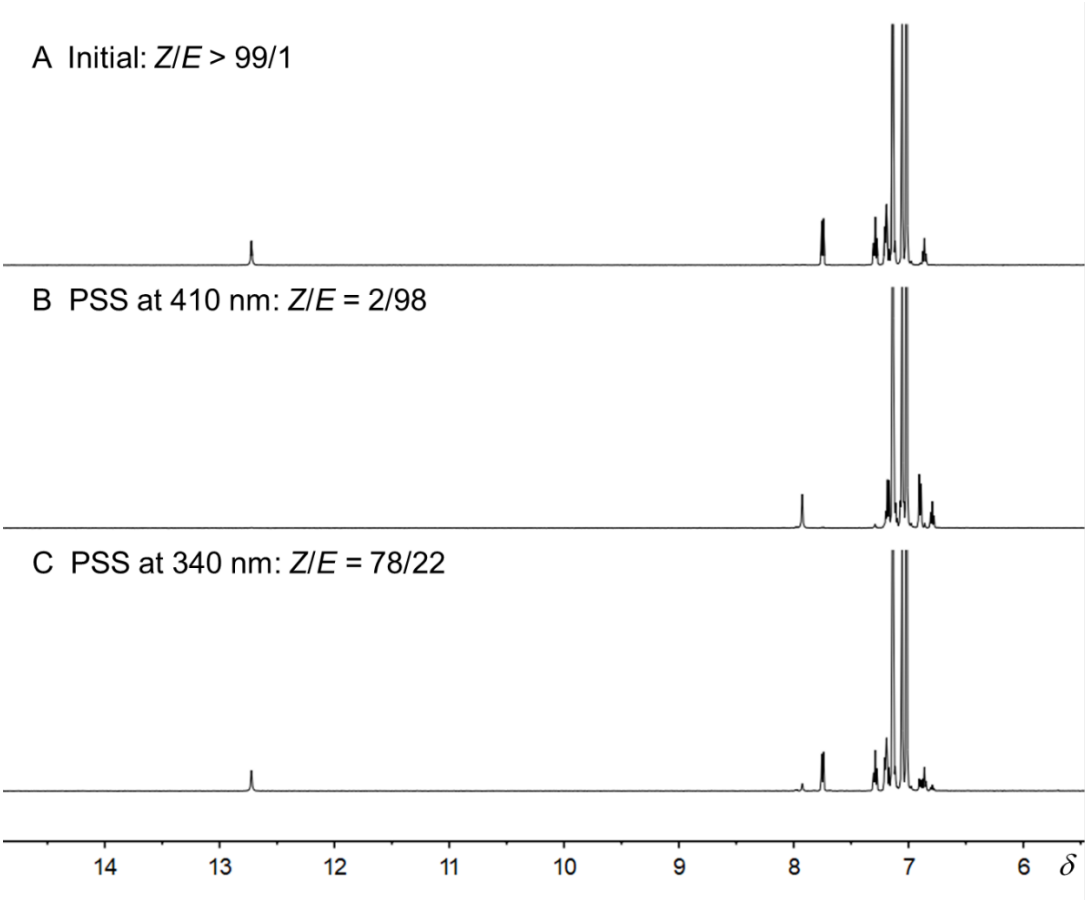

Figure S20. ^{1}H NMR spectra (toluene-d_8, 298 K) of **C8 HAT** (A) before, and after (B) 410 nm followed by (C) 340 nm photo irradiation to reach the PSS.

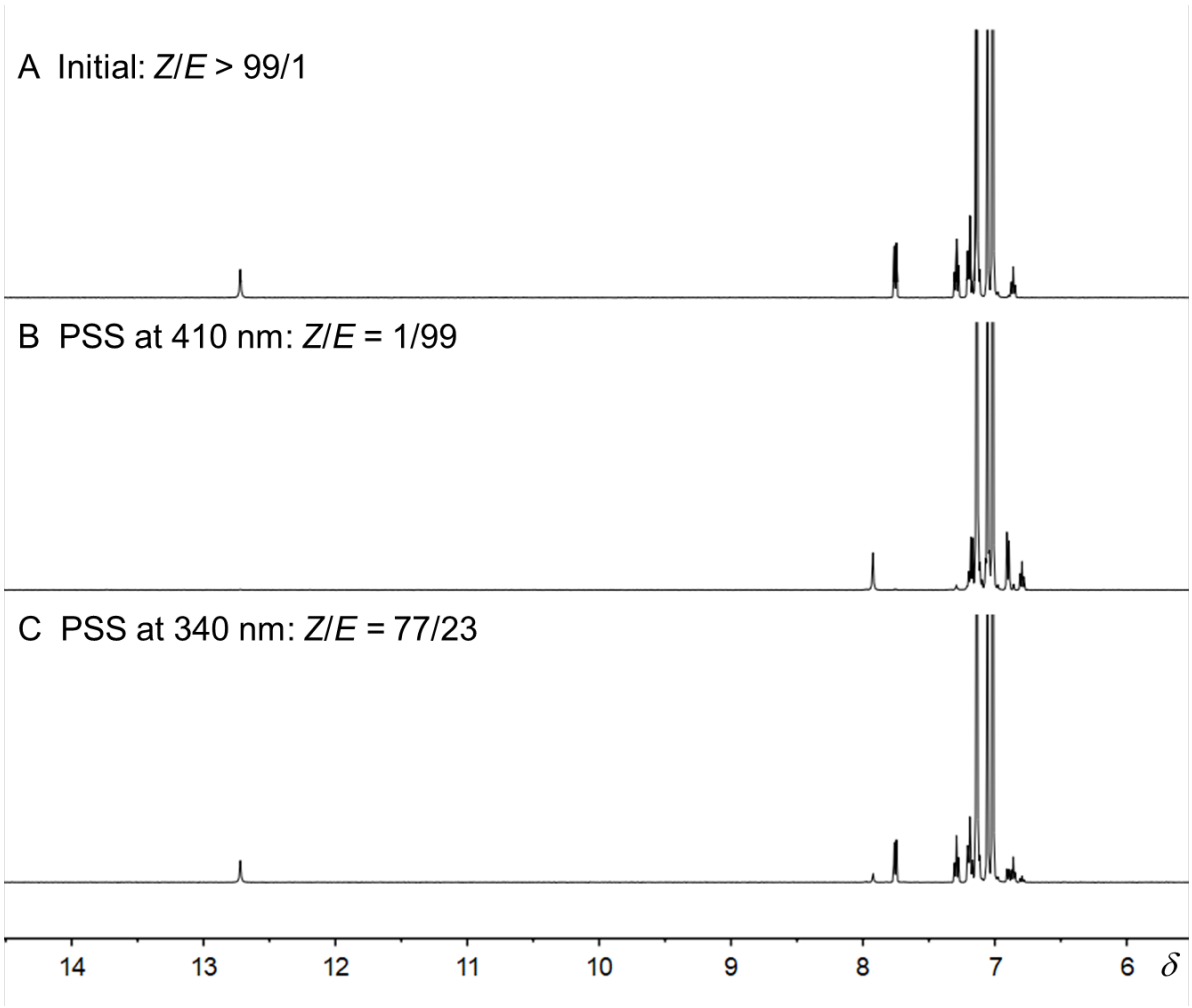

Figure S21. ^{1}H NMR spectra (toluene-d_8, 298 K) of **C10 HAT** (A) before, and after (B) 410 nm followed by (C) 340 nm photo irradiation to reach the PSS.

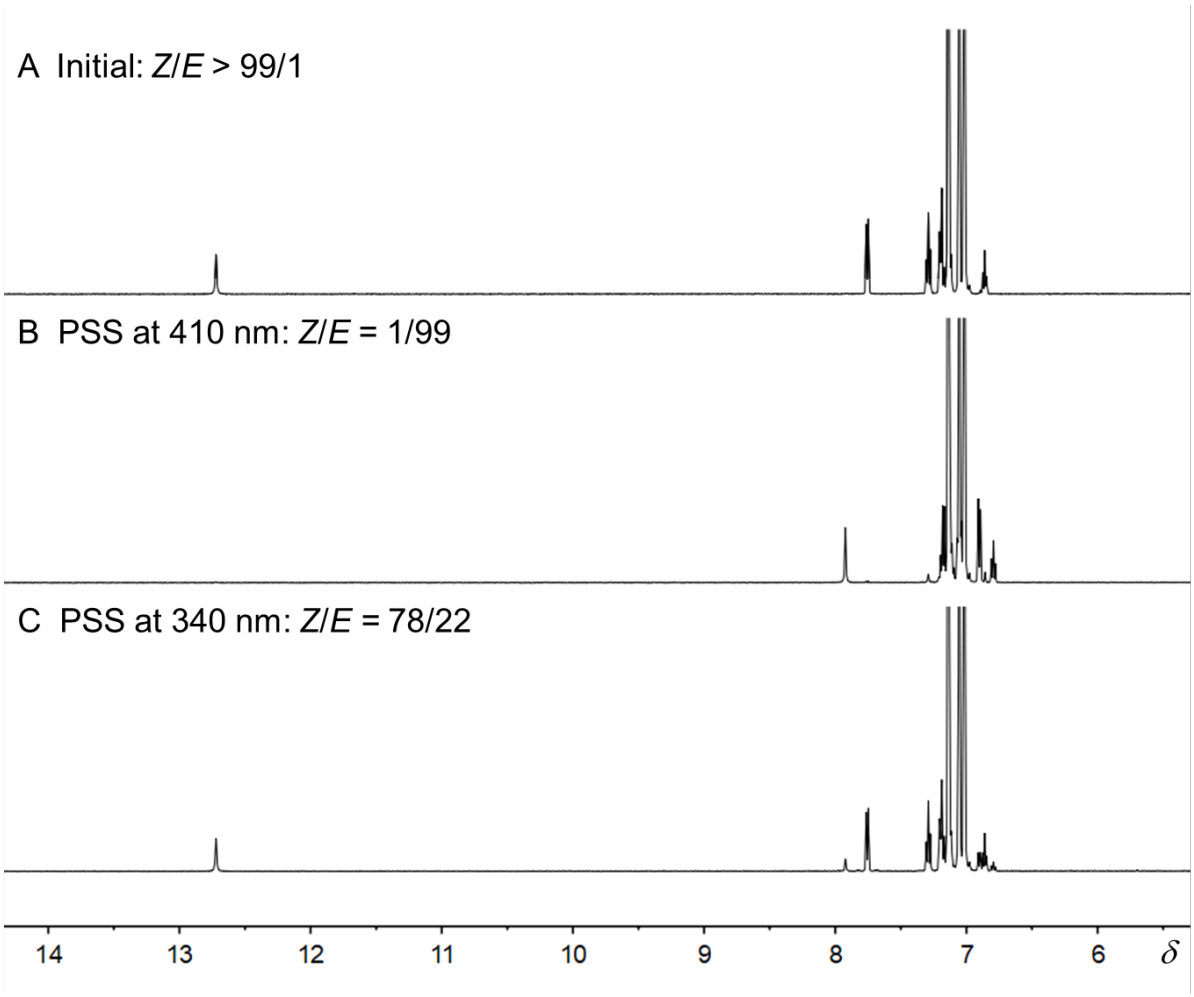

Figure S22. ^{1}H NMR spectra (toluene-d_8, 298 K) of **C11 HAT** (A) before, and after (B) 410 nm followed by (C) 340 nm photo irradiation to reach the PSS.

2.3 Photoisomerization Quantum Yield

The molar photon flux I_0 at 340 and 410 nm were determined using chemical actinometry.[S2] A 0.5 mL (= V_0) solution of potassium ferrioxalate in 0.05 M H_2SO_4 was placed into a 1.0 cm cuvette and irradiated for 30 seconds (= t_0). The irradiated solution was combined with 3.5 equiv. of ferrozine and stirred under dark for an hour. The resulting solution, containing reddish-purple $[Fe(ferrozine)_3]^{2+}$ complex was diluted by a factor of n, and its absorbance was measured at 563 nm (A_{563}), where its molar absorption coefficient (ε_{563}) is 27,900 cm^{-1} M^{-1}. The molar photon flux of the light source at different wavelengths was determined using Eq. 1.

$$I_0\left(quanta \cdot s^{-1}\right) = \frac{A_{563} \cdot n \cdot N_A \cdot V_0}{\varepsilon_{563} \cdot l \cdot t_0 \cdot \phi_\lambda} \qquad \text{Eq. 1}$$

where *l* indicates the length of cuvette; ϕ_λ stands for the quantum yield of the photo-reduction of Fe(III) oxalate induced by the light source (ϕ_{340} = 1.25, ϕ_{410} = 1.14); and N_A stands for Avogadro's number.

The photoisomerization quantum yields of hydrazone **1** were measured according to a previously reported method.[S2]

$$A \underset{k_r}{\overset{k_f}{\rightleftharpoons}} B$$

In a photochemical reaction, species **A** absorbs light to generate the product **B**.

The rate law for the formation of species **A** is as follows:

$$C_A = \frac{C_{total} \cdot k_r}{k_f + k_r} + \frac{C_{total} \cdot k_f}{k_f + k_r} e^{-(k_f + k_r)t} \qquad \text{Eq. 2}$$

C_A is proportional to the absorbance of species **A**. An exponential fit of absorbance as a function of time gives the observed rate constant $k_{obs} = k_f + k_r$. For hydrazone switch **1**, the thermal relaxation is slow at room temperature (Fig. S13) so $k_{A \to B} \approx k_{obs.}$

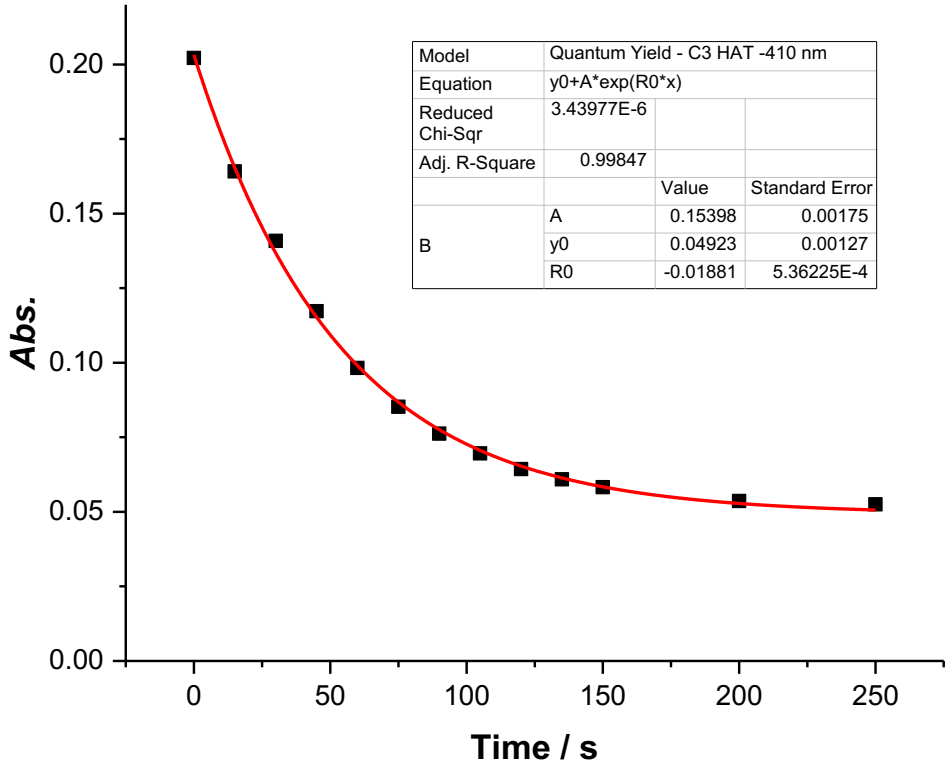

Figure S23. Kinetics for the photoisomerization (irradiation at 410 nm) of **C3 HAT**-*Z* to **C3 HAT**-*E* in toluene (1×10^{-5} M) at 298 K; the plot is of the absorbance (λ= 368 nm) as a function of time. $\varepsilon_{\textbf{C3 HAT-}Z@410\ nm}$ = 5200 $M^{-1} \cdot cm^{-1}$ was used for quantum yield calculations. The photoisomerization quantum yield was calculated to be 3.3 ± 0.2 % based on three consecutive measurements.

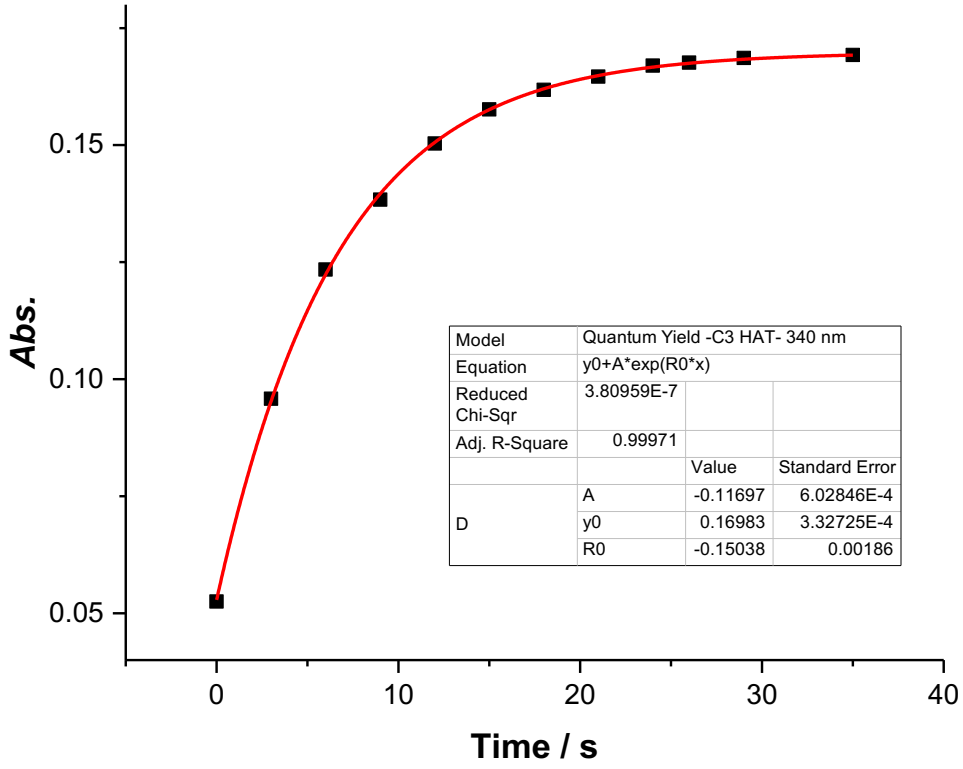

Figure S24. Kinetics for the photoisomerization (irradiation at 340 nm) of **C3 HAT**-*E* to **C3 HAT**-*Z* in toluene (1×10^{-5} M) at 298 K; the plot is of the absorbance (λ= 368 nm) as a function of time. $\varepsilon_{\textbf{C3 HAT-}E@340\ nm}$ = 17000 $M^{-1} \cdot cm^{-1}$ was used for quantum yield calculations. The photoisomerization quantum yield was calculated to be 7.0 ± 0.4 % based on three consecutive measurements.

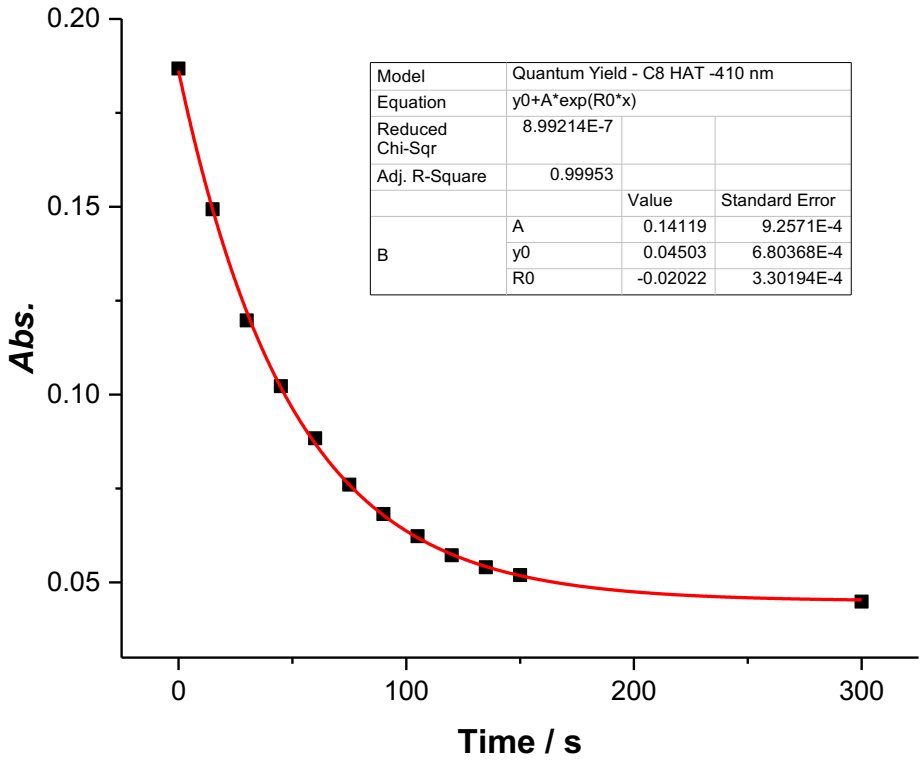

Figure S25. Kinetics for the photoisomerization (irradiation at 410 nm) of **C8 HAT**-*Z* to **C8 HAT**-*E* in toluene (1×10^{-5} M) at 298 K; the plot is of the absorbance (λ= 368 nm) as a function of time. $\varepsilon_{\textbf{C8 HAT-}Z@410\ nm}$ = 4500 $M^{-1} \cdot cm^{-1}$ was used for quantum yield calculations. The photoisomerization quantum yield was calculated to be 3.7 ± 0.1 % based on three consecutive measurements.

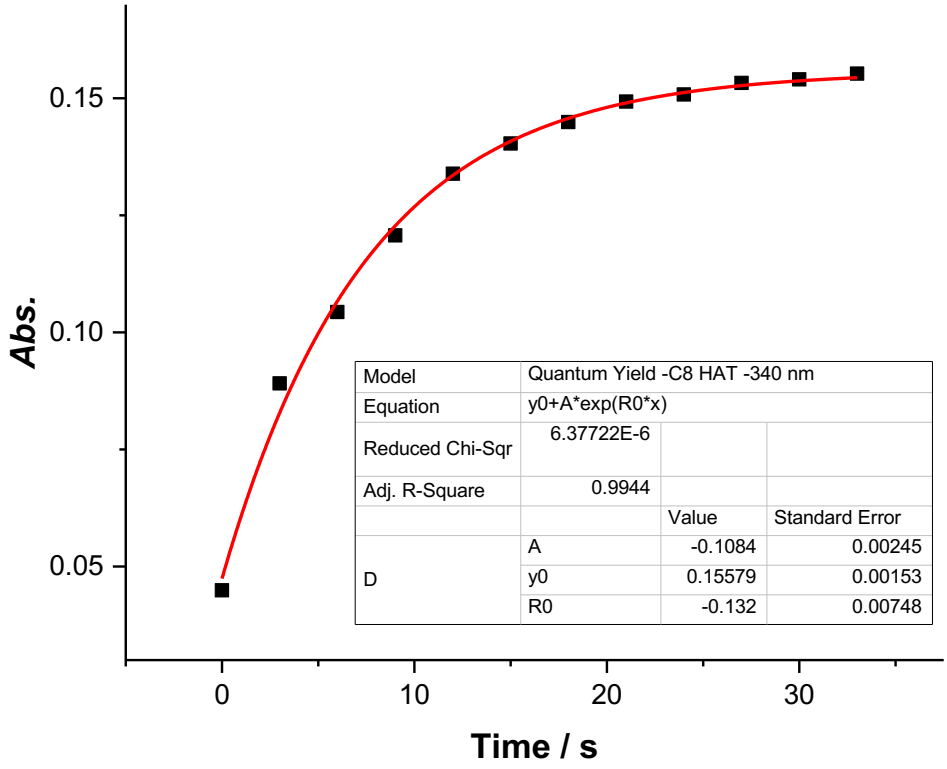

Figure S26. Kinetics for the photoisomerization (irradiation at 340 nm) of **C8 HAT**-*E* to **C8 HAT**-*Z* in toluene (1×10^{-5} M) at 298 K; the plot is of the absorbance (λ= 368 nm) as a function of time. $\varepsilon_{\textbf{C8 HAT-}E@340\ nm}$ = 15700 $M^{-1} \cdot cm^{-1}$ was used for quantum yield calculations. The photoisomerization quantum yield was calculated to be 6.9 ± 0.6 % based on three consecutive measurements.

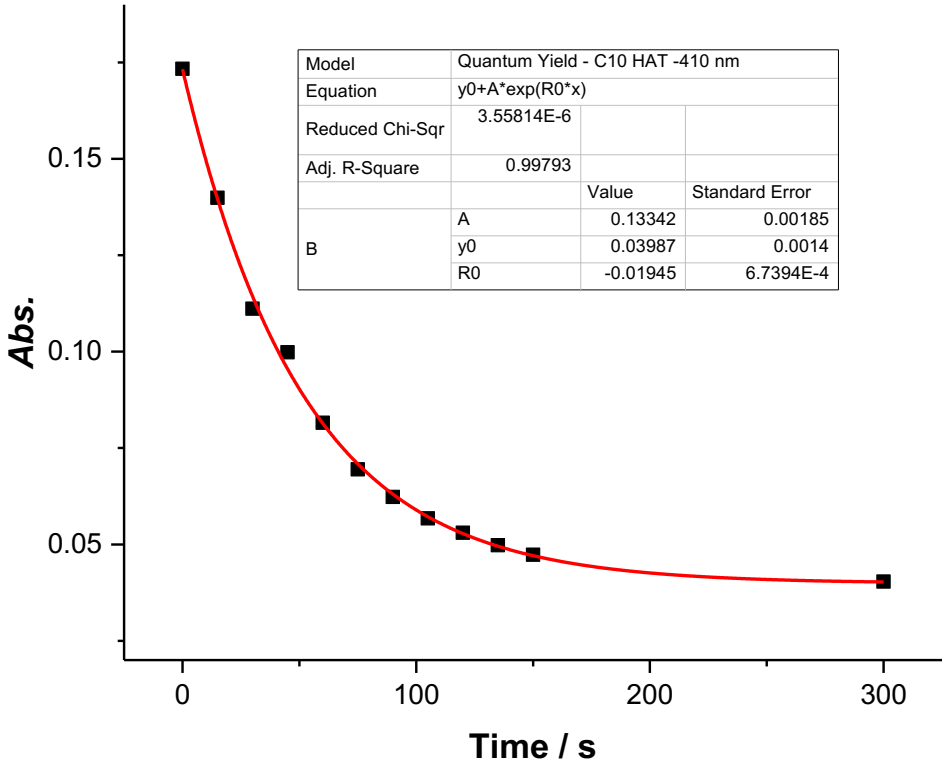

Figure S27. Kinetics for the photoisomerization (irradiation at 410 nm) of **C10 HAT**-*Z* to **C10 HAT**-*E* in toluene (1×10^{-5} M) at 298 K; the plot is of the absorbance (λ= 368 nm) as a function of time. $\varepsilon_{\textbf{C10 HAT-}Z@410\ nm}$ = 4100 $M^{-1} \cdot cm^{-1}$ was used for quantum yield calculations. The photoisomerization quantum yield was calculated to be 4.1 ± 0.1 % based on three consecutive measurements.

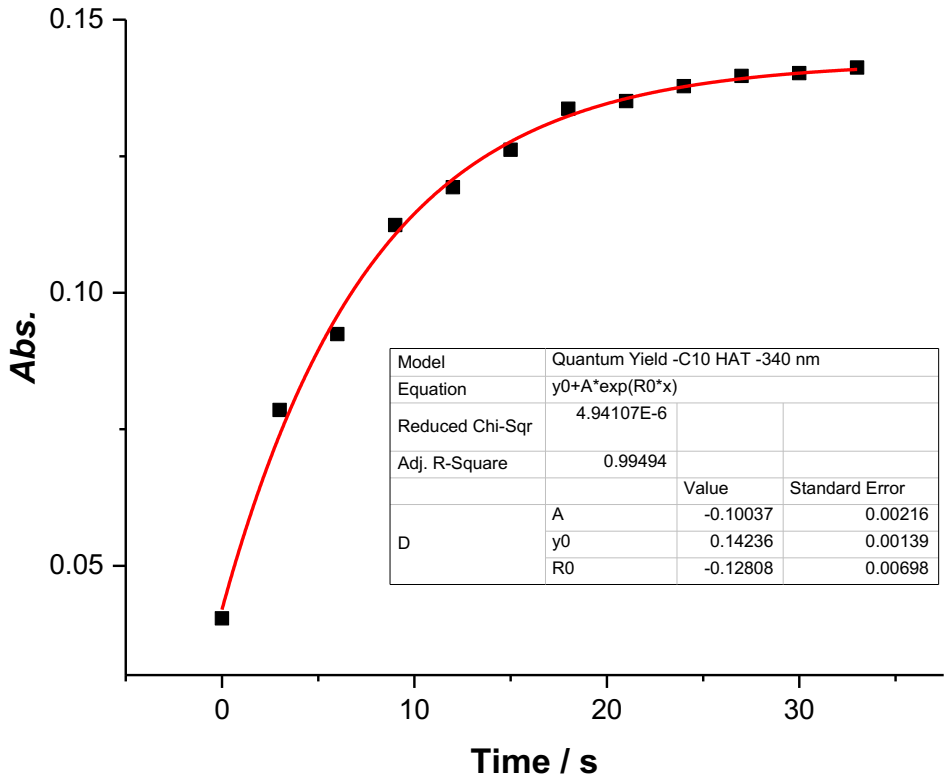

Figure 28. Kinetics for the photoisomerization (irradiation at 340 nm) of **C10 HAT**-*E* to **C10 HAT**-*Z* in toluene (1×10^{-5} M) at 298 K; the plot is of the absorbance (λ= 368 nm) as a function of time. $\varepsilon_{\textbf{C10 HAT-}E@340\ nm}$ = 14300 $M^{-1} \cdot cm^{-1}$ was used for quantum yield calculations. The photoisomerization quantum yield was calculated to be 8.3 ± 0.7 % based on three consecutive measurements.

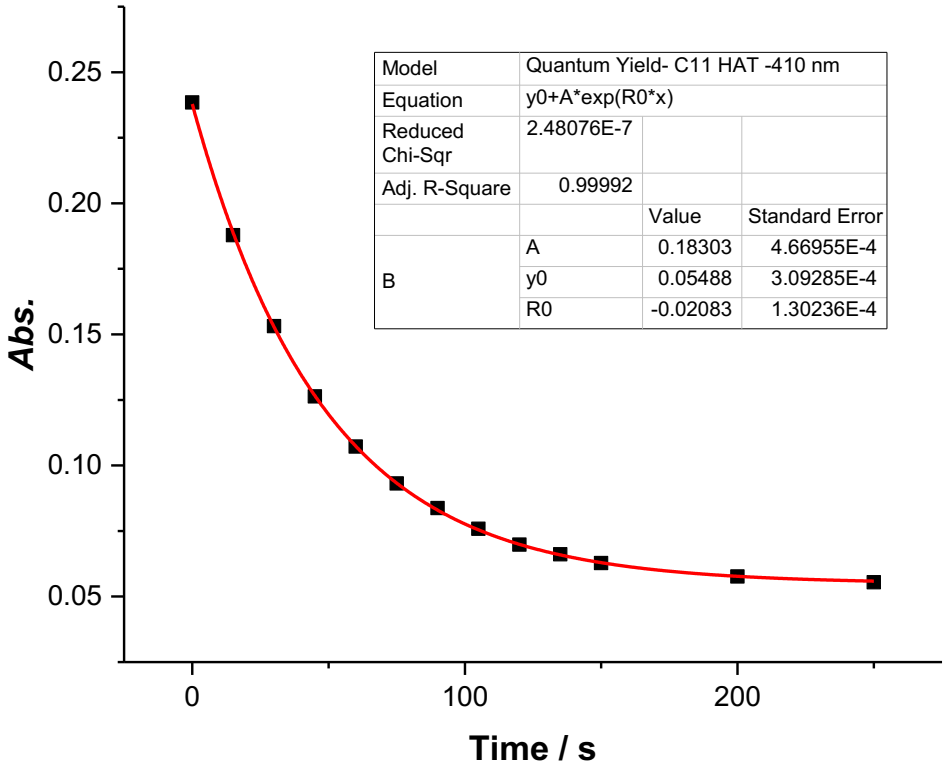

Figure S29. Kinetics for the photoisomerization (irradiation at 410 nm) of **C11 HAT**-*Z* to **C11 HAT**-*E* in toluene (1×10^{-5} M) at 298 K; the plot is of the absorbance (λ= 368 nm) as a function of time. $\varepsilon_{\textbf{C11 HAT-}Z@410\ nm}$ = 5700 $M^{-1} \cdot cm^{-1}$ was used for quantum yield calculations. The photoisomerization quantum yield was calculated to be 3.0 ± 0.1 % based on three consecutive measurements.

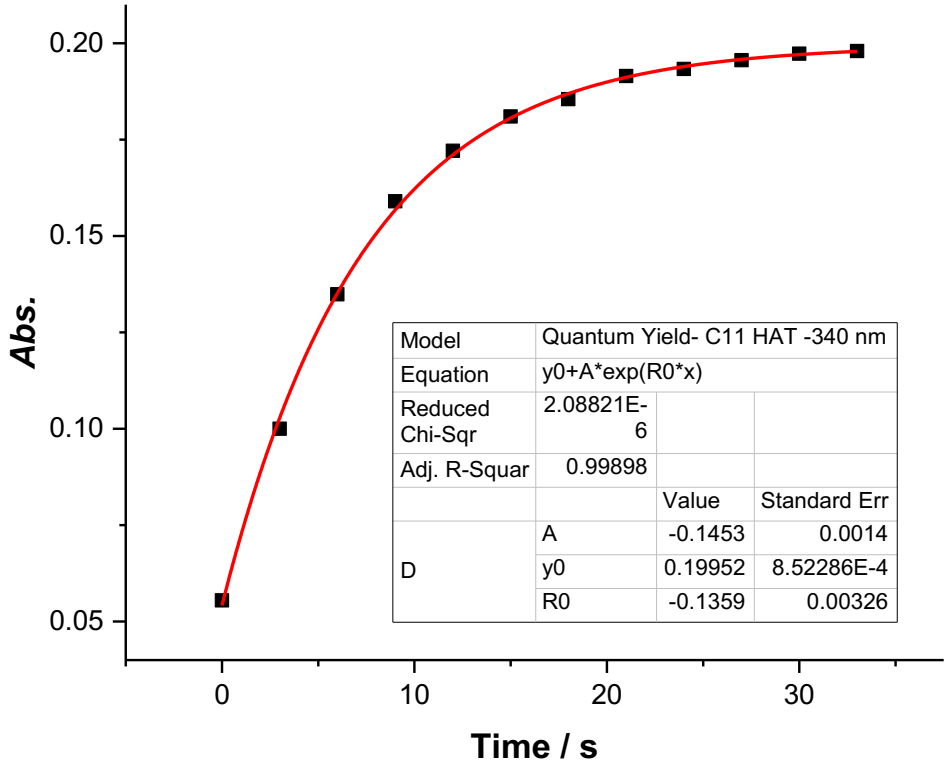

Figure S30. Kinetics for the photoisomerization (irradiation at 340 nm) of **C11 HAT**-*E* to **C11 HAT**-*Z* in toluene (1×10^{-5} M) at 298 K; the plot is of the absorbance (λ= 368 nm) as a function of time. $\varepsilon_{\textbf{C11 HAT-}E@340\ nm} = 20000\ M^{-1} \cdot cm^{-1}$ was used for quantum yield calculations. The photoisomerization quantum yield was calculated to be 5.6 ± 0.2 % based on three consecutive measurements.

2.4 Kinetic studies

The model compound **Cn Br** was used to estimate the thermal half-life of **Cn HAT** by following a reported procedure. [S3] A solution of **Cn Br** (1×10^{-3} M) in toluene-d_8 was prepared and then irradiated at 410 nm to obtain a *E* rich solution, which was then heated at 90 ºC under dark. The change in concentration of the *E* isomer as a function of time was monitored Half-life based on three measurements are listed below.

Table S2. Summary of the rate of $E \rightarrow Z$ relaxation at 363 K, energy barrier and half-life at 298 K.

Hydrazone	Run #	$k_{363\,K}$ (s^{-1})	$\Delta G^{\neq}$ (kJ mol^{-1})	$\tau_{1/2}$ (years)	$\overline{\tau_{1/2}}$ (years)
	1	9.41E-07	131	304	
C_3 Br	2	1.09E-06	130	253	250 ± 46
	3	1.36E-06	130	193	
	1	9.19E-07	131	313	
C_8 Br	2	8.42E-07	131	349	331 ± 15
	3	8.78E-07	131	331	
	1	7.42E-07	132	407	
C_{10} Br	2	7.44E-07	132	405	370 ± 51
	3	9.61E-07	131	297	
	1	1.24E-06	130	218	
C_{11} Br	2	1.57E-06	130	164	196 ± 23
	3	1.29E-06	130	208	

3. Simulated and confocal Raman spectra of Cn HAT

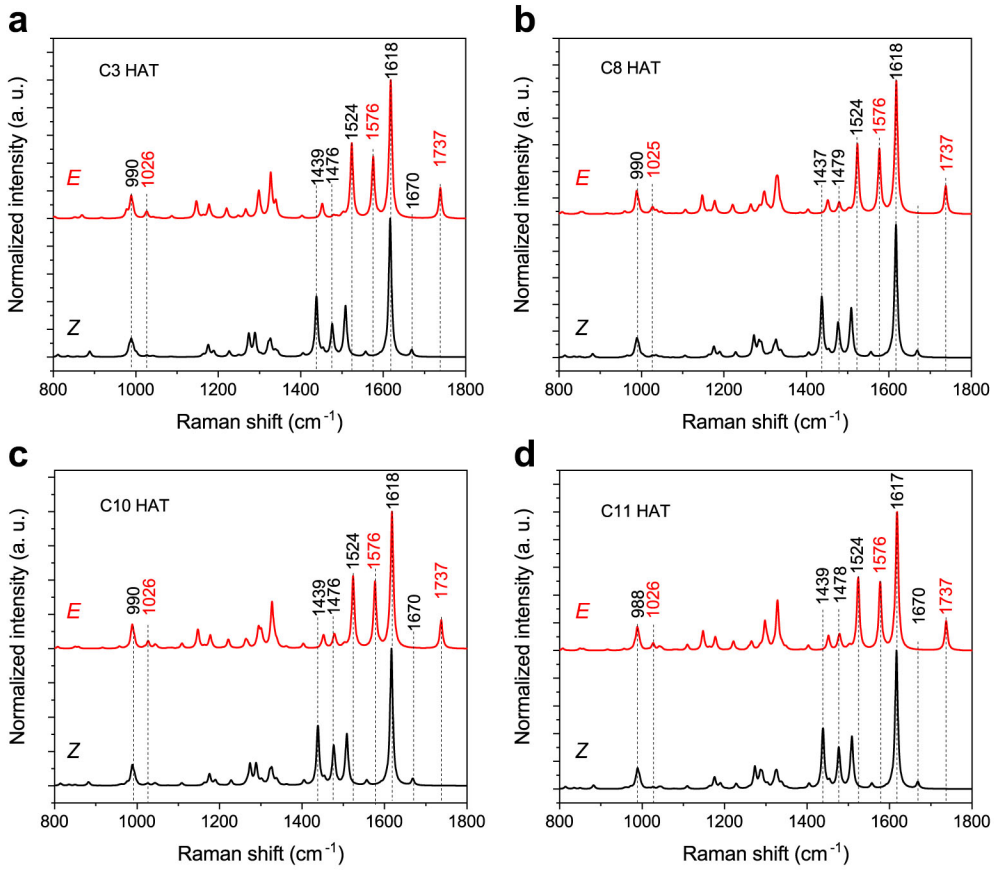

Figure S31. Simulated Raman spectra of the *Z* (black curve) and *E* isomers (red curve) of Cn HAT (n = 3, 8, 10, 11). (**a**) C3 HAT; (**b**) C8 HAT; (**c**) C10 HAT; (**d**) C11 HAT.

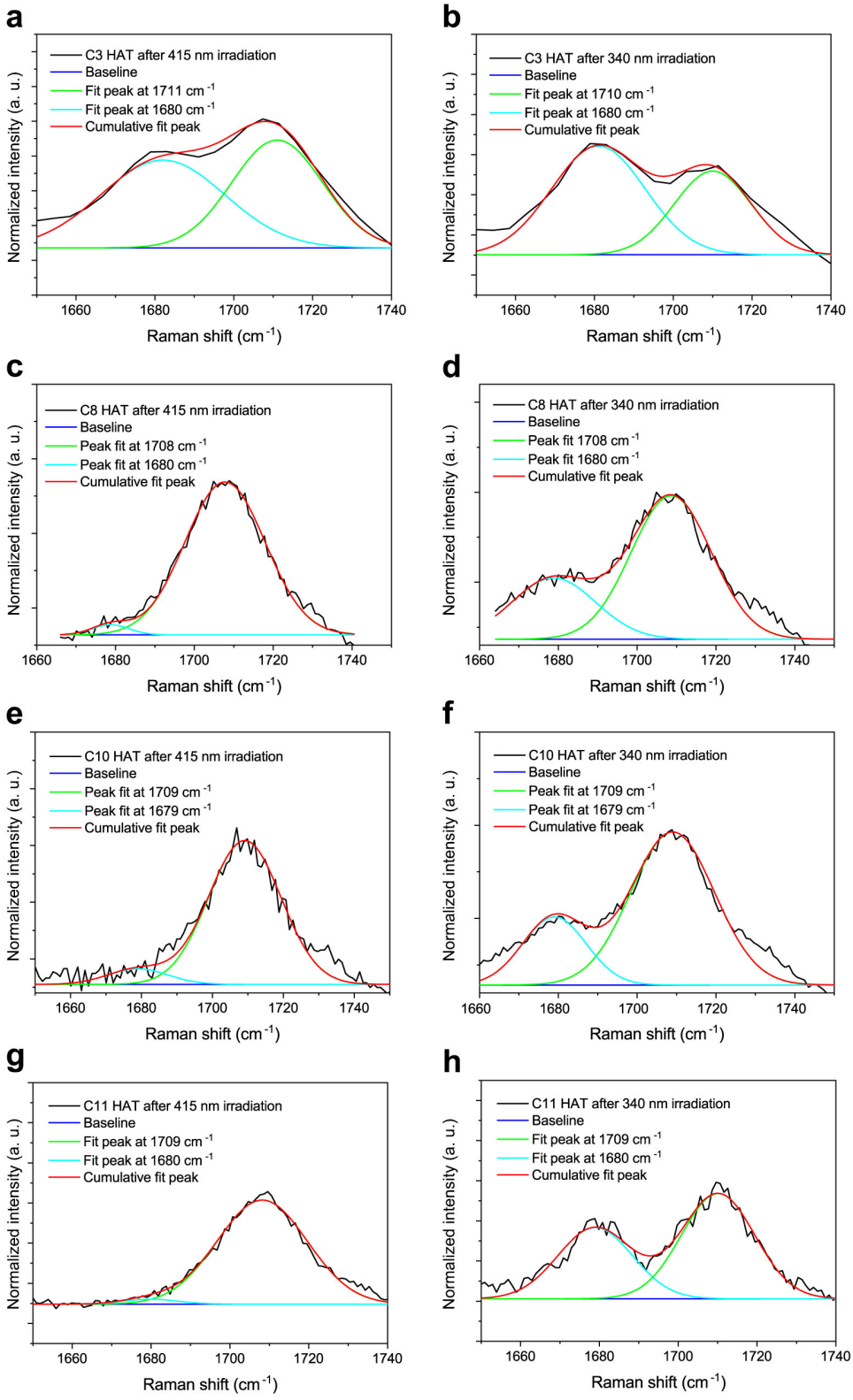
a
C3 HAT after 415 nm irradiation
Baseline
Fit peak at 1711 cm -1
Fit peak at 1680 cm -1
Cumulative fit peak
b
C3 HAT after 340 nm irradiation
Baseline
Fit peak at 1710 cm -1
Fit peak at 1680 cm -1
Cumulative fit peak
c
C8 HAT after 415 nm irradiation
Baseline
Peak fit at 1708 cm -1
Peak fit at 1680 cm -1
Cumulative fit peak
d
C8 HAT after 340 nm irradiation
Baseline
Peak fit 1708 cm -1
Peak fit 1680 cm -1
Cumulative fit peak
e
C10 HAT after 415 nm irradiation
Baseline
Peak fit at 1709 cm -1
Peak fit at 1679 cm -1
Cumulative fit peak
f
C10 HAT after 340 nm irradiation
Baseline
Peak fit at 1709 cm -1
Peak fit at 1679 cm -1
Cumulative fit peak
g
C11 HAT after 415 nm irradiation
Baseline
Fit peak at 1709 cm -1
Fit peak at 1680 cm -1
Cumulative fit peak
h
C11 HAT after 340 nm irradiation
Baseline
Fit peak at 1709 cm -1
Fit peak at 1680 cm -1
Cumulative fit peak
Normalized intensity (a. u.)
Raman shift (cm -1)
1660
1680
1700
1720
1740

Figure S32. Gaussian curve fit of the confocal Raman spectrum of Cn HAT (with Raman shift ranging from 1650-1750 cm^{-1}) after irradiation with 415 nm light (**a, c, e, g**), followed by irradiation with 340 nm light (**b, d, f, h**), (**a, b**) C3 HAT; (**c, d**) C8 HAT; (**e, f**) C10 HAT; (**g, h**) C11 HAT.

Table S3. Photochemical properties of Cn HAT (n = 3, 8, 10, 11) powders

Parameter	C3 HAT	C8 HAT	C10 HAT	C11 HAT
([*E*]:[*Z*])$_{PSS415}$ (%)	48:52	97:3	92:8	97:3
([*E*]:[*Z*])$_{PSS340}$ (%)	39:61	71:29	75:25	59:41

4. UV-vis spectroscopy results of Cn HAT SAMs on Au

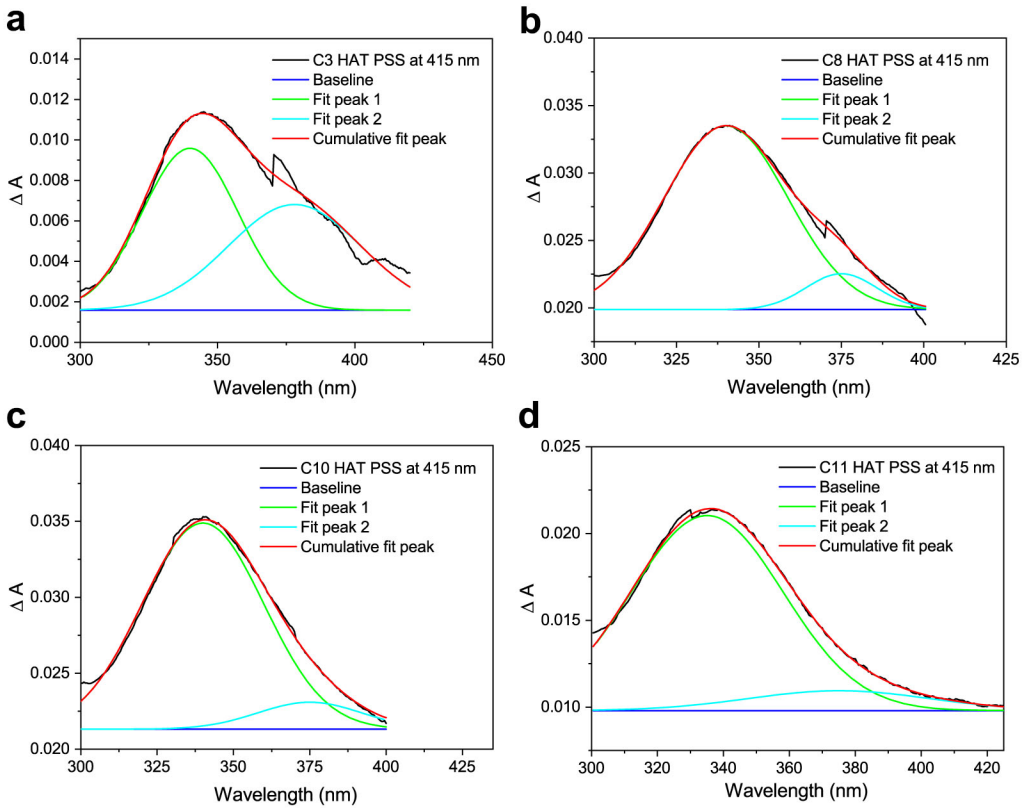

Figure S33. Gaussian curve fit of the UV-vis spectrum of Cn HAT self-assembled monolayer (SAM) on Au after irradiation with 415 nm light, (**a**) C3 HAT; (**b**) C8 HAT; (**c**) C10 HAT; (**d**) C11 HAT.

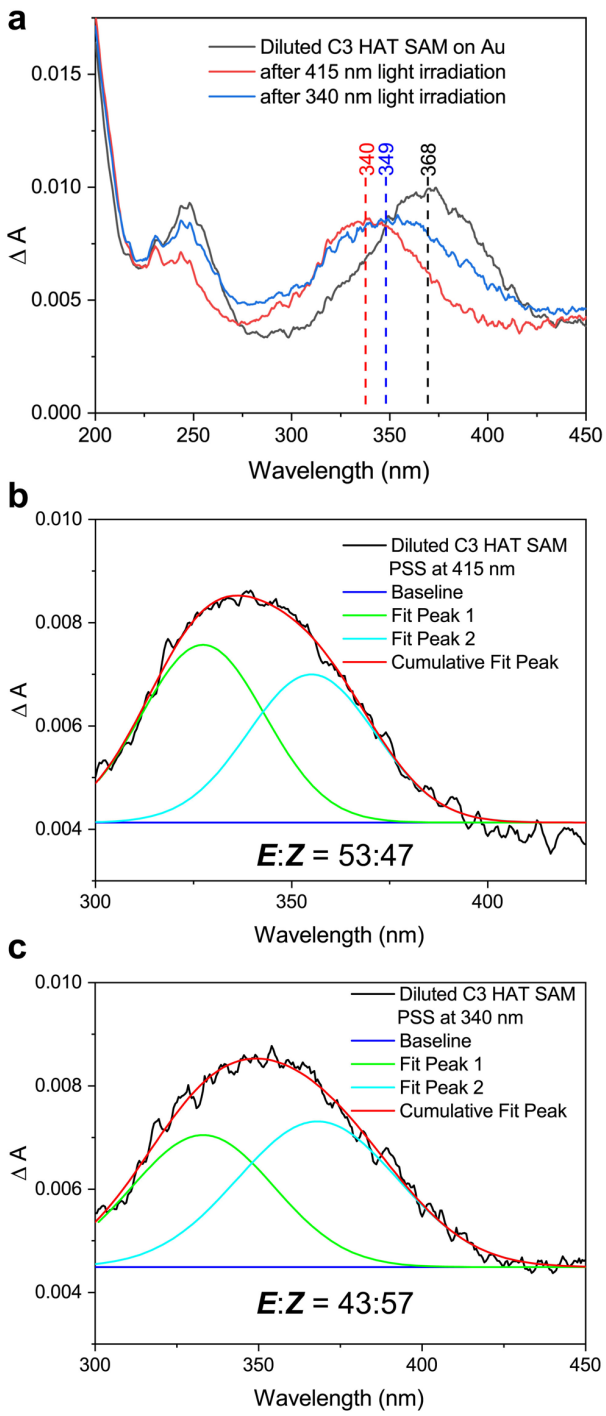

Figure S34. a. UV-Vis spectroscopy of C3 HAT on Au diluted with propanethiol before (black curve) and after (red curve) 415 nm light irradiation, followed by irradiation with 340 nm light (blue curve). b/c. Gaussian curve fit of the UV-vis spectra of C3 HAT on Au diluted with propanethiol after irradiation with 415 nm light (b), followed by irradiation with 340 nm light (c). The y axis (Δ A) represents the absorbance of Cn HAT SAMs, the absorbance of the Au substrate has been subtracted from the total absorbance of Cn HAT SAMs on Au.

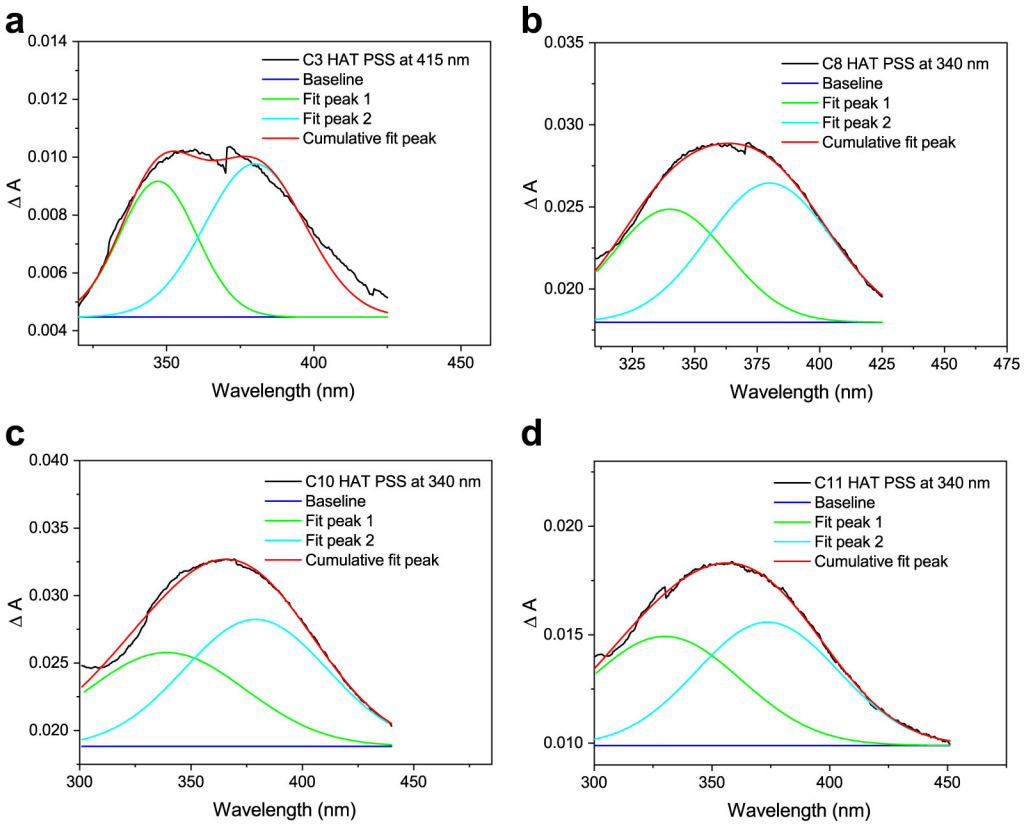

Figure S35. Gaussian curve fit of the UV-vis spectrum of Cn HAT self-assembled monolayers (SAMs) on Au after irradiation with 415 nm light, followed by irradiation with 340 nm light. (**a**) C3 HAT; (**b**) C8 HAT; (**c**) C10 HAT; (**d**) C11 HAT.

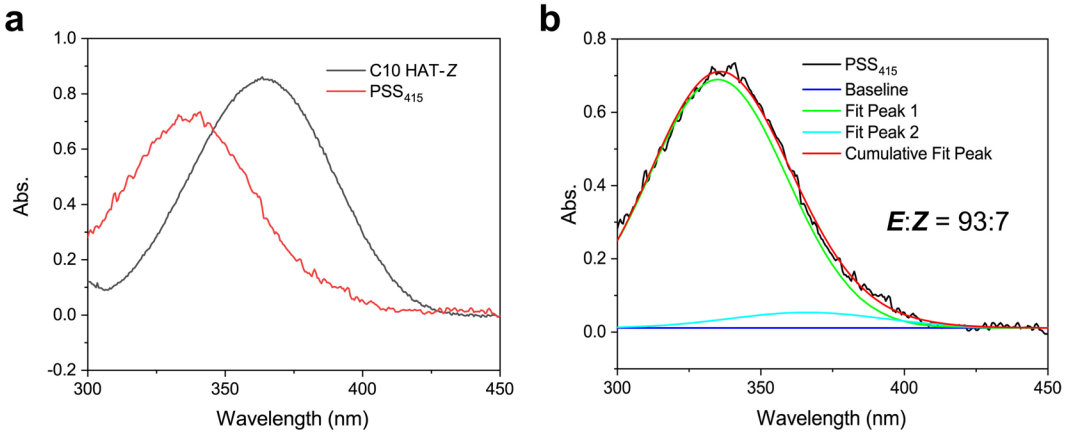

Figure S36. UV-Vis spectroscopy of C10 HAT dissolved in EtOH before (black curve) and after (red curve) 415 nm light irradiation. b. Gaussian curve fit of the UV-vis spectra of C10 HAT in EtOH after irradiation with 415 nm light.

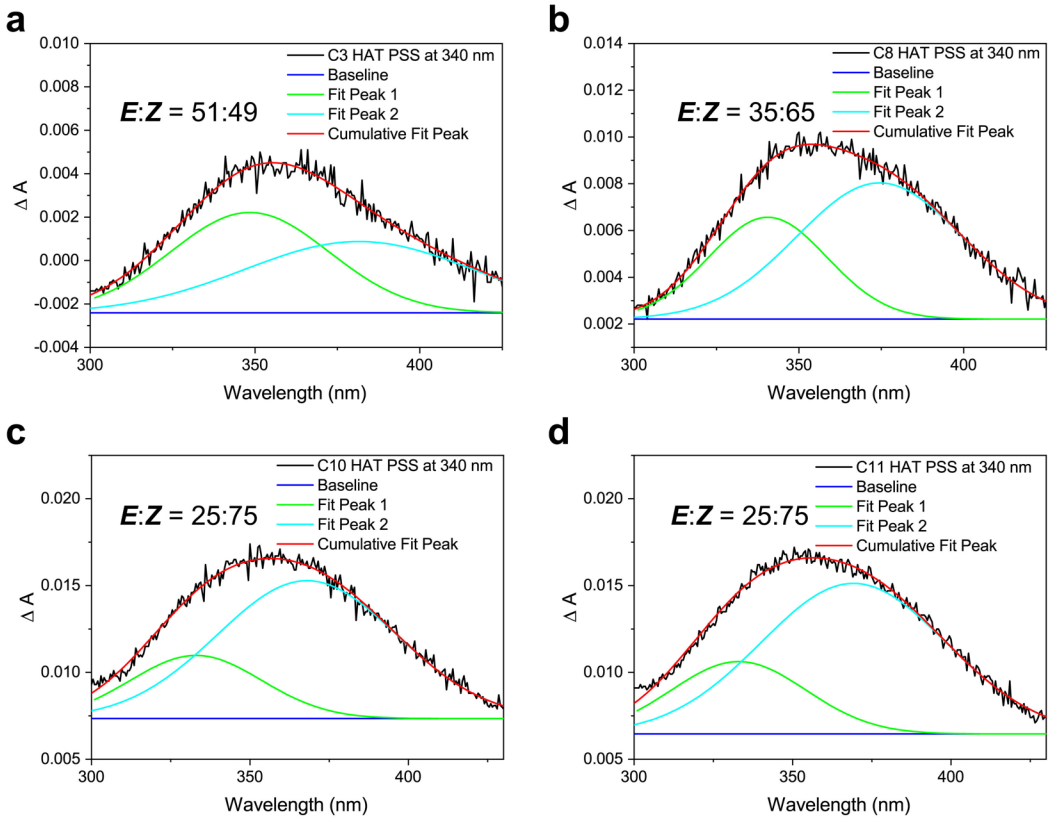

Figure S37. Gaussian curve fit of the UV-vis spectrum of *E*-C*n* HAT SAMs on Au after irradiation with 340 nm light. (**a**) C3 HAT; (**b**) C8 HAT; (**c**) C10 HAT; (**d**) C11 HAT.

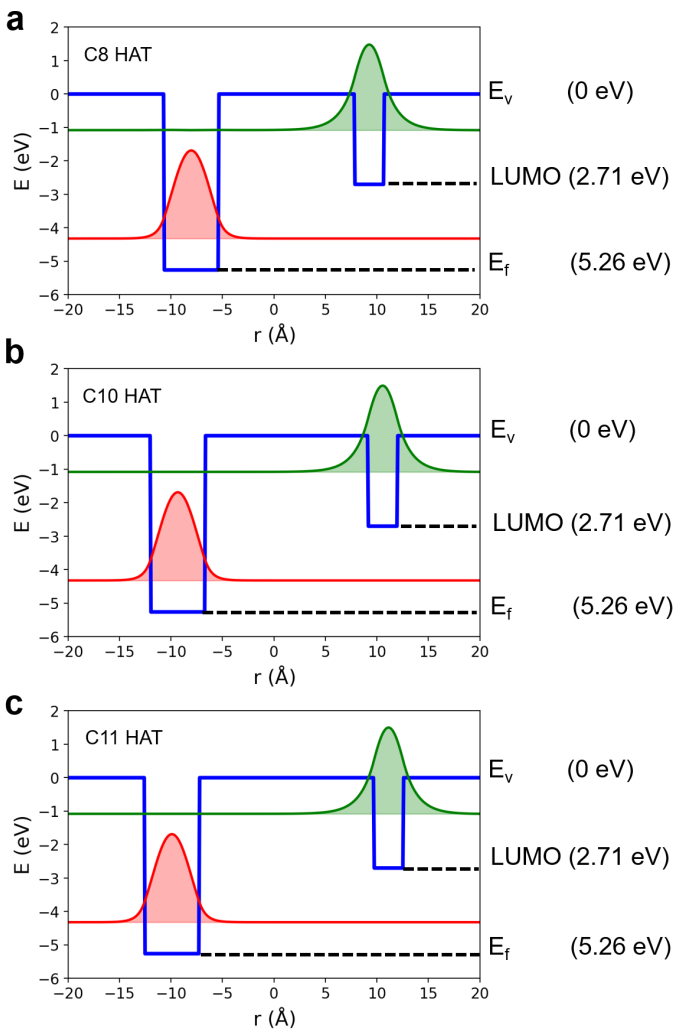

Figure S38. The solution of one-dimensional double-well model for C8 HAT (a), C10 HAT (b), and C11 HAT (c) on Au.

One-dimensional double-well model

The charge transfer can be modeled as a particle in a box. In this case, the depth of the potential well corresponds to their energy level vs. vacuum (E_v = 0 eV). The excitation energy is obtained as the energy difference between the ground state and the first excited state of the described Schrödinger equation under Dirichlet boundary conditions.

$$\left[-\frac{\hbar^2}{2m}\nabla^2 + V(x)\right]\Phi(x) = E\Phi(x)$$

Where V(r) is given by a double-well potential:

$$V(x) = \begin{cases} 0 & , \quad else \\ EA & , \quad -\frac{d}{2} - W_{mol} < x < -\frac{d}{2} \\ E_f - E_v & , \quad \frac{d}{2} < x < \frac{d}{2} + W_{metal} \end{cases}$$

Where EA is the electron affinity of the molecule adsorbed on the metal surface; E_f is the Fermi level, which can be obtained from DFT calculations. The potential wells are separated by the alkyl linker length of d, and the width of the potential wells are taken from the average distance between molecules on the Au surface (√3 a, a is the average bond length of Au-Au) and the length of the dihedral atoms (C-C=N-N, corresponding to the LUMO orbitals)

The probability of the electron distribution is calculated by the square of the wavefunction.

$$P = \int |\Phi(x)|^2 dx$$

Note that our model assumes that irradiation light can overcome the transition from d-band edge to Fermi level to ensure the Fermi level is occupied by the electron from the metal surface, as suggested by our previous work. [s1]

Table S4. Calculation results of C*n* HAT SAM on Au

Molecules	E_v (eV)	E_f (eV)	HOMO (eV)	LUMO (eV)	E_1-E_0 (eV)
C3 HAT	0	5.46	5.50	2.90	3.10
C8 HAT	0	5.26	5.36	2.71	3.02
C10 HAT	0	5.26	5.36	2.71	3.02
C11 HAT	0	5.26	5.36	2.71	3.02

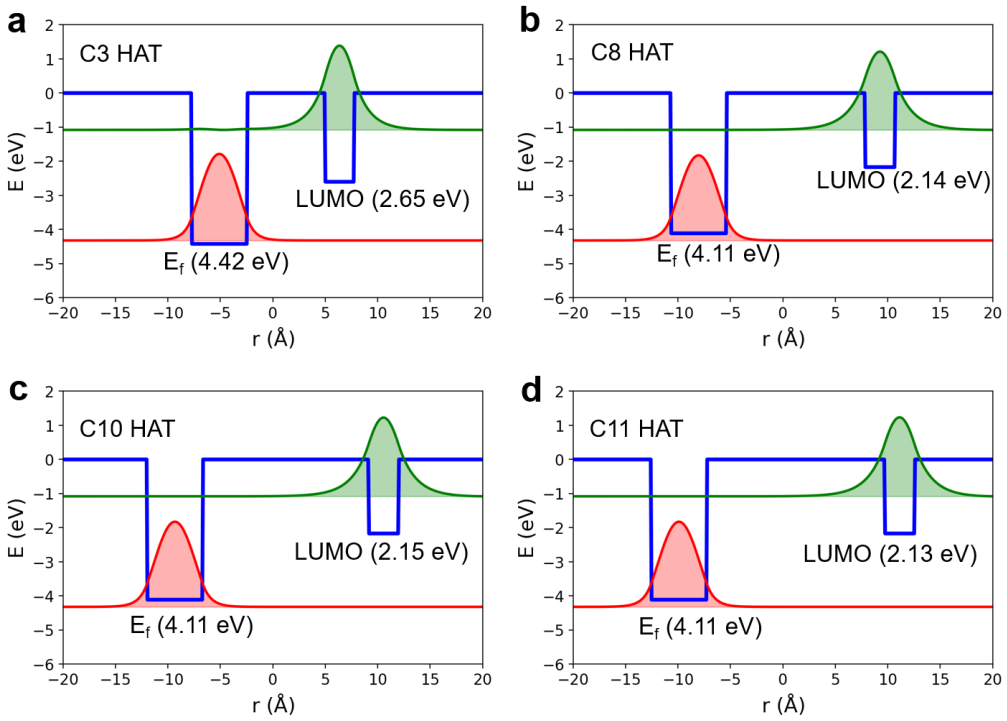

Figure S38. The solution of one-dimensional double-well model for C3 HAT (a), C8 HAT (b), C10 HAT (c), and C11 HAT (d) on Ag.

Table S5. Calculation results of C*n* HAT SAM on Ag

Molecules	E_v (eV)	E_f (eV)	HOMO (eV)	LUMO (eV)	E_1-E_0 (eV)
C3 HAT	0	4.42	5.26	2.65	2.31
C8 HAT	0	4.11	4.81	2.14	2.28
C10 HAT	0	4.11	4.81	2.15	2.28
C11 HAT	0	4.11	4.81	2.13	2.28

5. TERS study of the photoisomerization of Cn HAT SAMs on Au

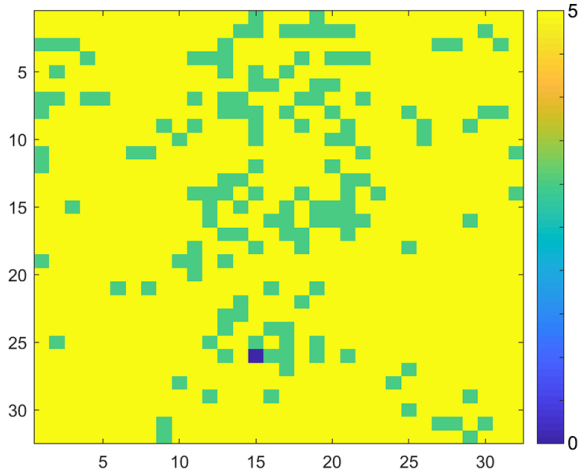

Figure S39. TERS map of the Raman peak intensity at 1573 cm^{-1} of a C8 HAT SAM on Au after irradiation with 415 nm light. The intensity of the peak is indicated as 0 when signal to noise ratio (S/N) is smaller than 3; it is indicated as 5 when S/N is bigger than 5. The size of the maps is 1 x 1 μm^2 with 32 nm pixel size. The peak at 1573 cm^{-1} appears in 85 % of the spectra in the map.

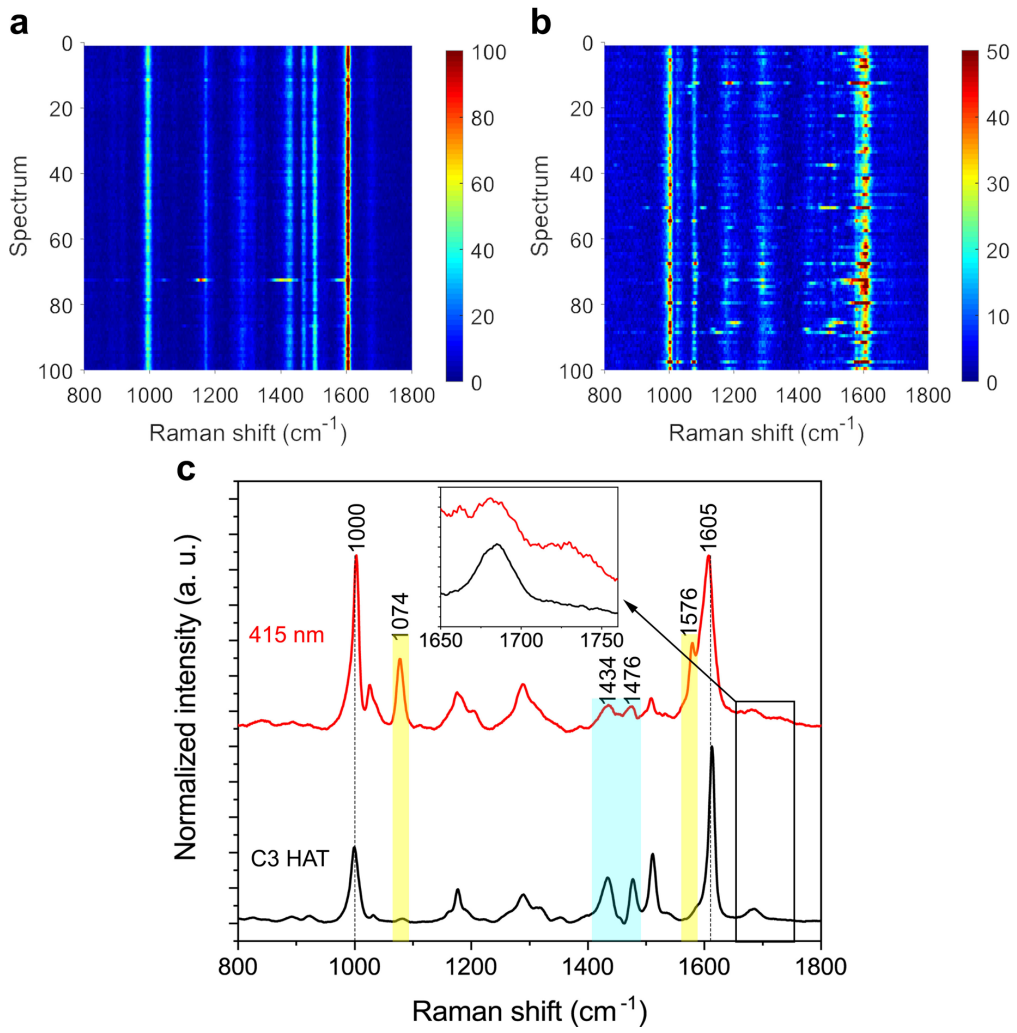

Figure S40. (**a**,**b**) Waterfall plot of all TER spectra from maps of a C3 HAT SAM on Au before (**a**) and after irradiation with 415 nm light (**b**). The size of all maps is 1 × 1 μm^2 with a 100 nm pixel size. (**c**) Averaged TER spectra of a C3 HAT SAM on Au surface before (black curve) and after irradiation with 415 nm light (red curve). The peaks at 1434 and 1476 cm^{-1} marked with a blue rectangle correspond to the *Z* isomer. The peaks at 1074 and 1576 cm^{-1} marked with yellow rectangles correspond to the *E* isomer. All TER spectra were normalized to the Raman peak at 1605 cm^{-1}.

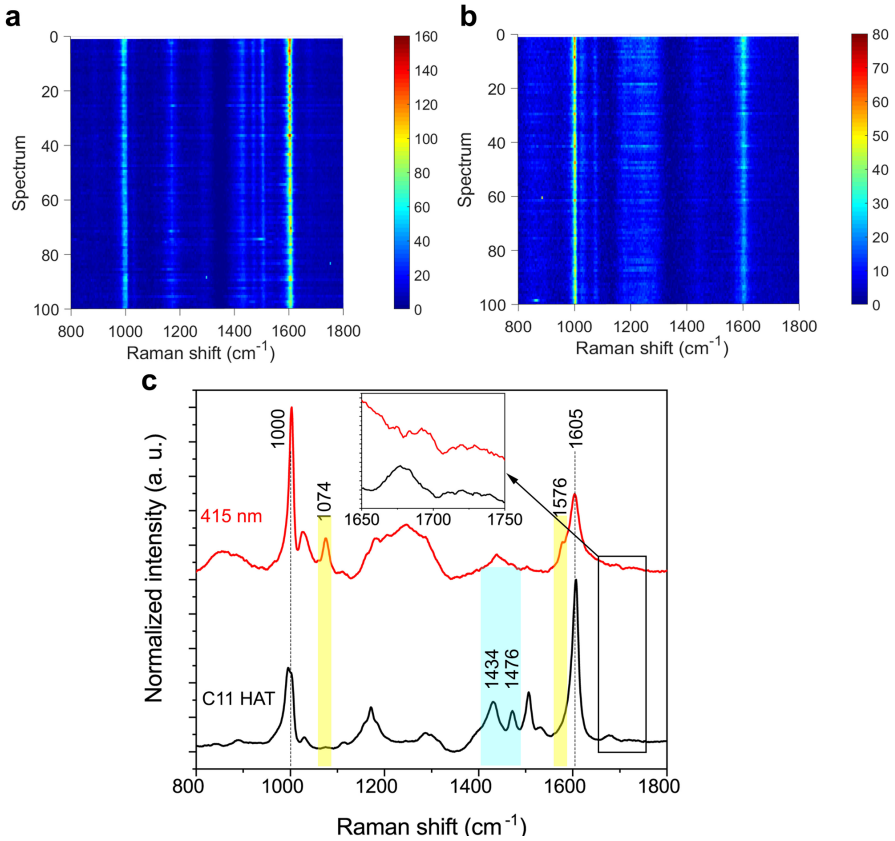

Figure S41. (**a**,**b**) Waterfall plot of all TER spectra from maps of a C11 HAT SAM on Au before (**a**) and after irradiation with 415 nm light (**b**). The size of all maps is 1 × 1 μm^2 with a 100 nm pixel size. (**c**) Averaged TER spectra of a C11 HAT SAM on Au surface before (black curve) and after irradiation with 415 nm light (red curve). The peaks at 1434 and 1476 cm^{-1} marked with a blue rectangle correspond to the *Z* isomer. The peaks at 1074 and 1576 cm^{-1} marked with yellow rectangles correspond to the *E* isomer. All TER spectra were normalized to the Raman peak at 1605 cm^{-1}.

6. UV-vis spectroscopy results of Cn HAT SAMs on Ag

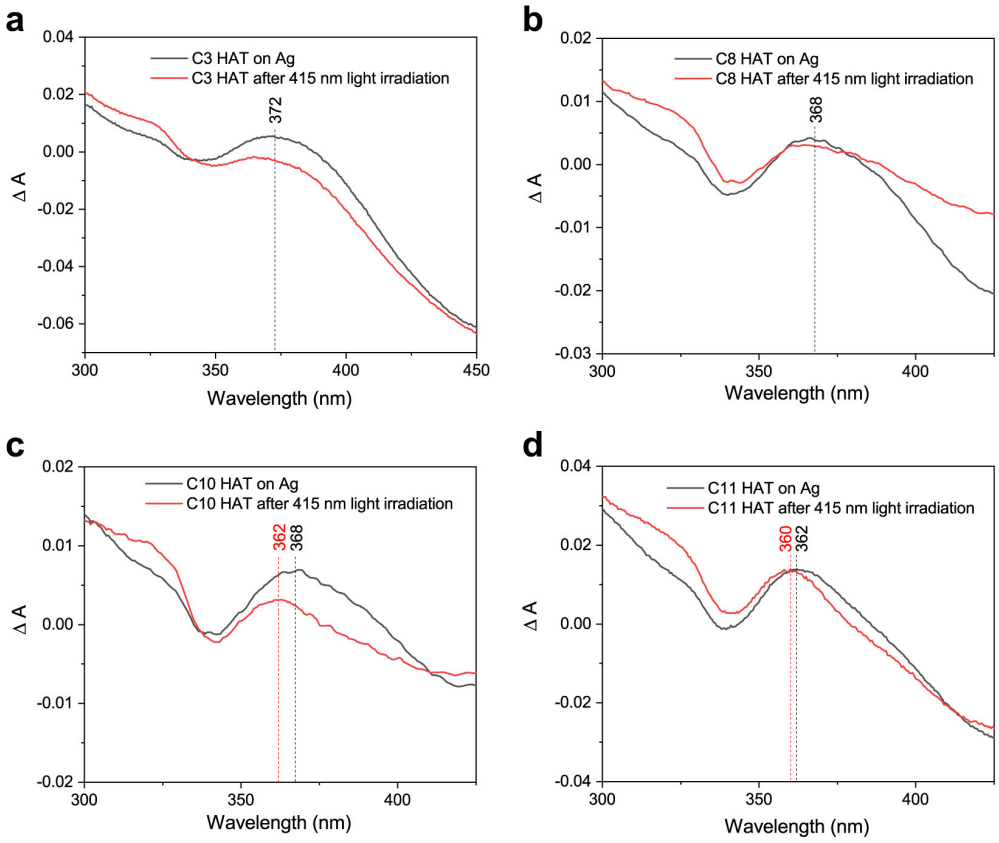

Figure S42. UV-vis spectra of Cn HAT (n = 3, 8, 10, 11) SAMs on Ag before (black curve) and after irradiation with 415 nm light (red curve), (**a**). C3 HAT; (**b**). C8 HAT; (**c**). C10 HAT; (**d**). C11 HAT. The y axis (Δ A) represents the absorbance of Cn HAT SAMs, the absorbance of the Ag substrate has been subtracted from the total absorbance of Cn HAT SAMs on Ag. The negative absorbance shown in the Figures is due to the imperfect subtraction of the absorbance of Ag.

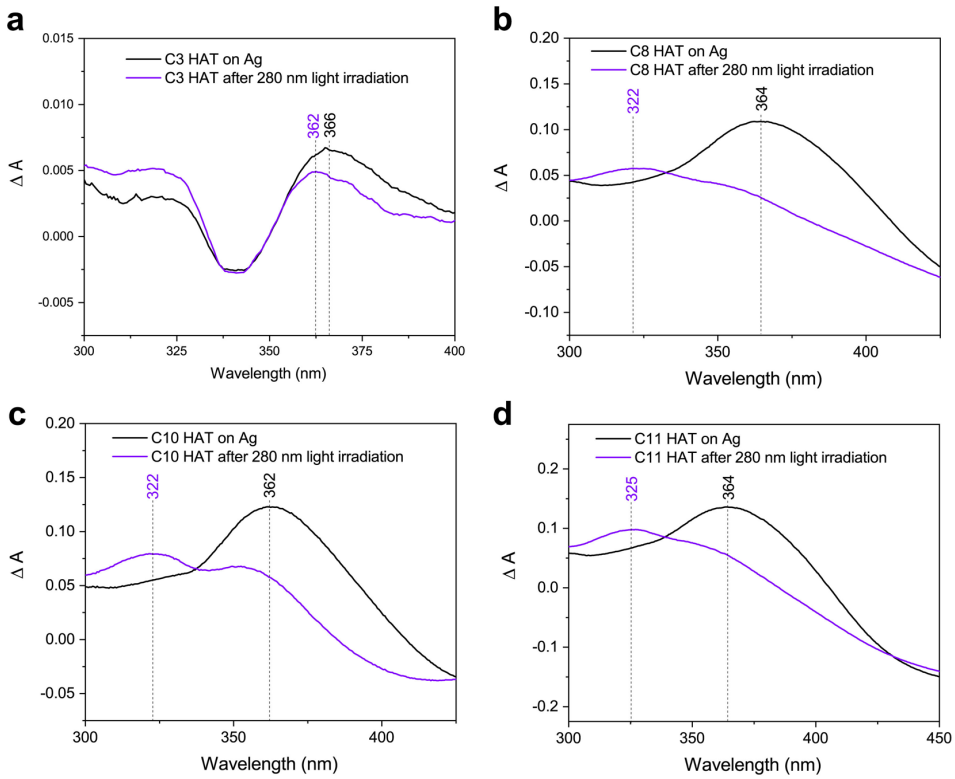

Figure S43. UV-vis spectra of Cn HAT (n = 3, 8, 10, 11) SAMs on Ag before (black curve) and after irradiation with 280 nm light (purple curve), (**a**). C3 HAT; (**b**). C8 HAT; (**c**). C10 HAT; (**d**). C11 HAT. The y axis (Δ A) represents the absorbance of Cn HAT SAMs, the absorbance of the Ag substrate has been subtracted from the total absorbance of Cn HAT SAMs on Ag. The negative absorbance shown in the Figures is due to the imperfect subtraction of the absorbance of Ag.

7. References

[S1] L.-Q. Zheng, S. Yang, J. Lan, L. Gyr, G. Goubert, H. Qian, I. Aprahamian, R. Zenobi. *J. Am. Chem. Soc.* **2019,** *141*, 17637-17645.

[S2] (a) H. J. Kuhn, S. E. Braslavsky, R. Schmidt. *Pure Appl. Chem.* **2004**, *76*, 2105-2146; (b) H. M. D Bandara, T. R. Friss, M. M. Enriquez, W. Isley, C. Incarvito, H. A. Frank, J. Gascon, S. C. Burdette. *J. Org. Chem.* **2010**, *75*, 4817-4827.

[S3] H. Qian, S. Pramanic, I. Aprahamian. *J. Am. Chem. Soc.* **2017**, *139*, 9140-9143.